was implanted on the left-hand side as a control. Fentanyl citrate was infused during and after the surgery. After the surgery, the dogs were treated with analgesics (butorphanol tartrate, 0.2mg/kg, im) and a tapered dose of dexamethasone (0.5–0.1mg/kg, iv) and antibiotics (cefazolin, 20mg/kg, im) for 3 days.

CT analysis

Bone formation inside and around the implants was regularly assessed by CT until the dogs were euthanized. The CT value Hounsfield Unit (HU) was measured at the designated point representing the body of the implant and the cylindrical holes (Fig. 3B). These assessments were performed under sedation using midazolam (0.3mg/kg, im) and medetomidine (20μg/kg, im).

Histological procedures

Experimental animals were euthanized by injection of a deep anesthetic dose of thiopental sodium followed by KCl solution at 24 weeks after the implantation. The implanted region, including the surrounding tissue, was excised and fixed in 10% phosphate-buffered formalin for 7 days and decalcified in 10% Ethylenediaminetetracetic acid for 7 weeks. After fixation, the decalcified specimens were embedded in paraffin. Seven-micrometer sections were cut and stained with hematoxylin and eosin for morphological analysis, with Masson's trichrome for detection of bone tissue, or with tartrate-resistant acid phosphatase staining for visualization of osteoclasts.

Results

Implant materials

TIs were fabricated by a 3D ink-jet printer (Fig. 1) using CAD data based on CT data (Fig. 2A). Figure 2B shows a photograph of a TI. The bending strength of the TI was 8.2MPa and the compressive strength was 18.6MPa, which is comparable to those of HI (9 and 20MPa, respectively). The TI was easily manipulated with a round bar (Dentsply, Tokyo) to finely adjust its shape. In contrast, it was difficult and time-consuming to cut the HI with a round bar because of its brittleness. No major adverse effects related to the implants were observed. A slight increase in serum alkaline phosphatase (ALP) was observed at 8 weeks after implantation, the reason for which is unknown. Among isozymes, liver-specific ALP-2 was elevated.

Radiological evaluation

Analysis of the CT images revealed that the HU of the body part of the TI gradually increased (Fig. 3D). There was a rapid increased in HU for the cylindrical holes during the first 4 weeks and a gradual increase thereafter suggesting new bone formation at these sites. When we calculated the volume of the cylindrical holes, it had decreased by 60% at 24 weeks after the implantation. In contrast, there was no significant increase in HU in the HI-implanted group (Fig. 3C). Bony bridging, the HU of which was around 1000, was observed between the TIs and the temporal bone at 4 and 24 weeks after implantation, but no such bridging was observed in the HI-implanted group (Fig. 4).

Histological evaluation

Histological analysis using Masson's trichrome staining revealed that in both the TI- and HI-treated groups, mainly connective tissues invaded the body part of the implants (Fig. 5A–D). In contrast, massive invasion of bone tissue and bone marrow was observed in the cylindrical holes of

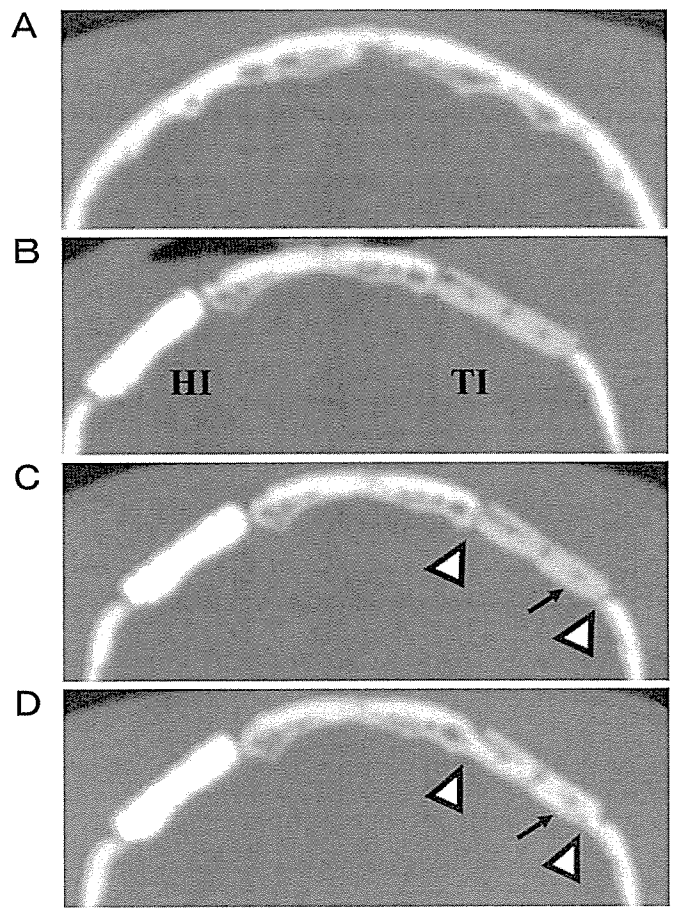

Fig. 4A–D. CT images of a beagle's skull at preimplantation (**A**), immediate postimplantation (**B**), 4 weeks after implantation (**C**), and 24 weeks after implantation (**D**). For the TI, the diameter of the cylindrical holes became narrowed (*arrows*). Bony bridging (*triangles*) between TI and the temporal bone was observed at 4 and 24 weeks postoperatively (**C** and **D**). *HI*, porous HA implant; *TI*, tailor-made TCP implant

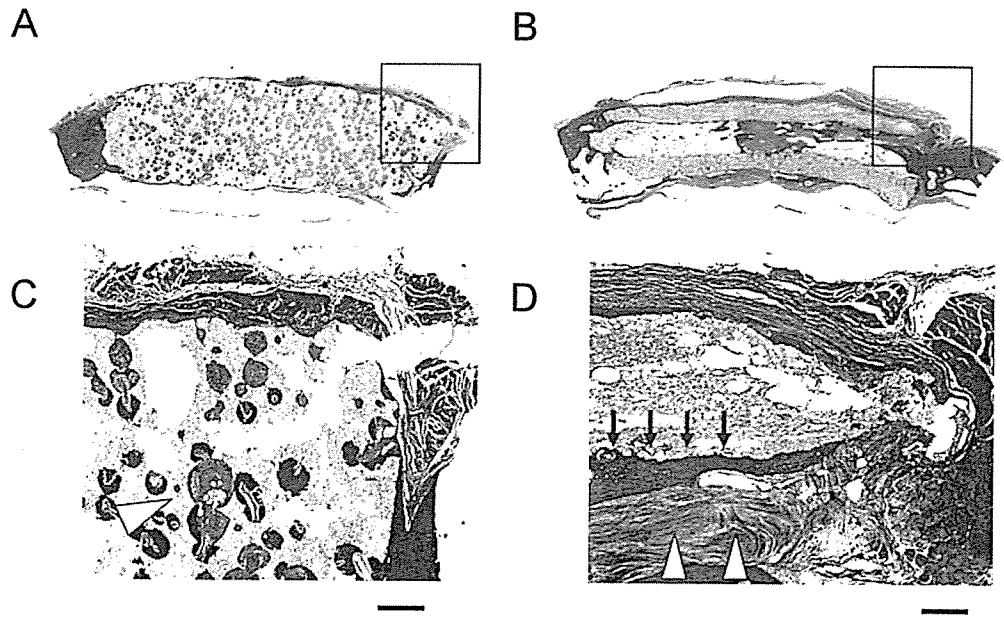

Fig. 5A–D. Masson's trichrome stain of the porous HA implant (**A** and **C**) and the tailor-made TCP implant (**B** and **D**) at 24 weeks after the implantation. For the porous HA block, collagen tissues comprising of mainly collagen fibers (*arrowheads*) were seen migrating into the porous structures (**A** and **C**). For the TI, both collagen tissue (*arrowheads*) and bone tissue (*arrows*) were seen migrating from the ends into the cylindrical holes (**B** and **D**). *Scale bar* 250 μm

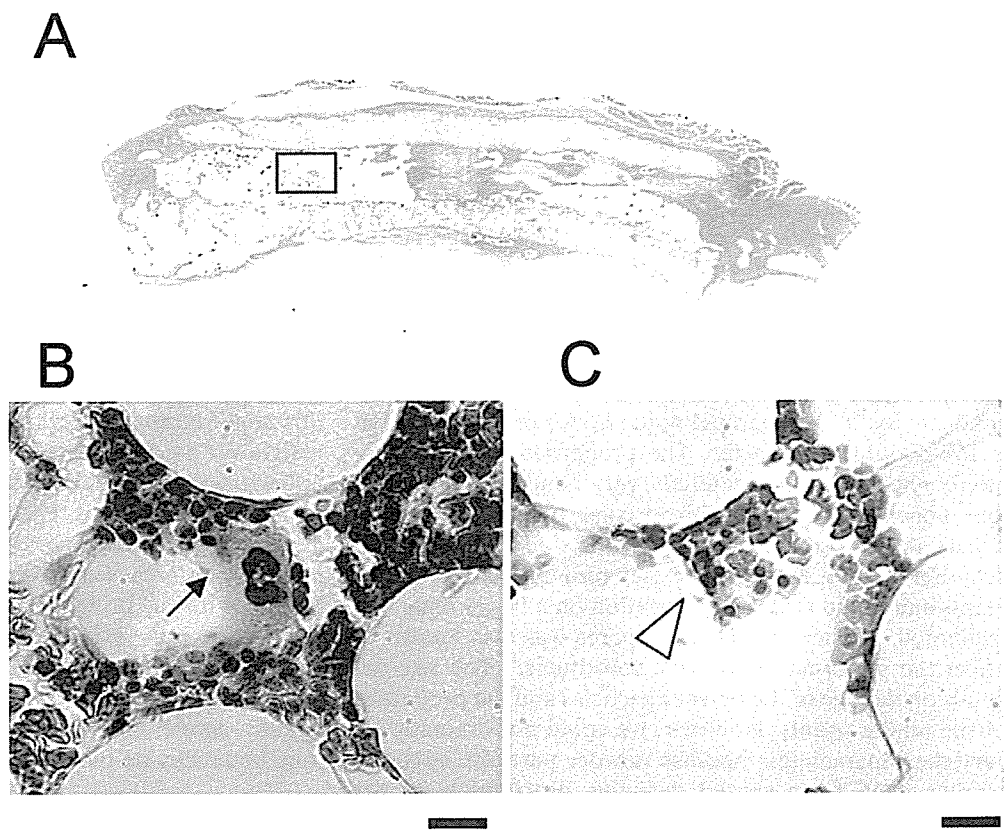

Fig. 6A–C. Hematoxylin and eosin stain of the cylindrical holes of the tailor-made TCP implant at 24 weeks after the implantation. Bone marrow formation occurred (**A**). At higher magnification, megakaryocytes (*arrow*) and erythroblasts (*arrowheads*) were seen (**B** and **C**). *Scale bar* 10 μm

the TI (Fig. 5B and D; Fig. 6), while only a small amount of bone tissue invaded the porous part of HI, with no formation of bone marrow. In TI, bone resorbing osteoclasts were observed in the porous part and also inside the cylindrical holes (Fig. 7).

Discussion

TIs were fabricated directly by an ink-jet printer. Ink-jet printing is well suited to generating complex shapes as well

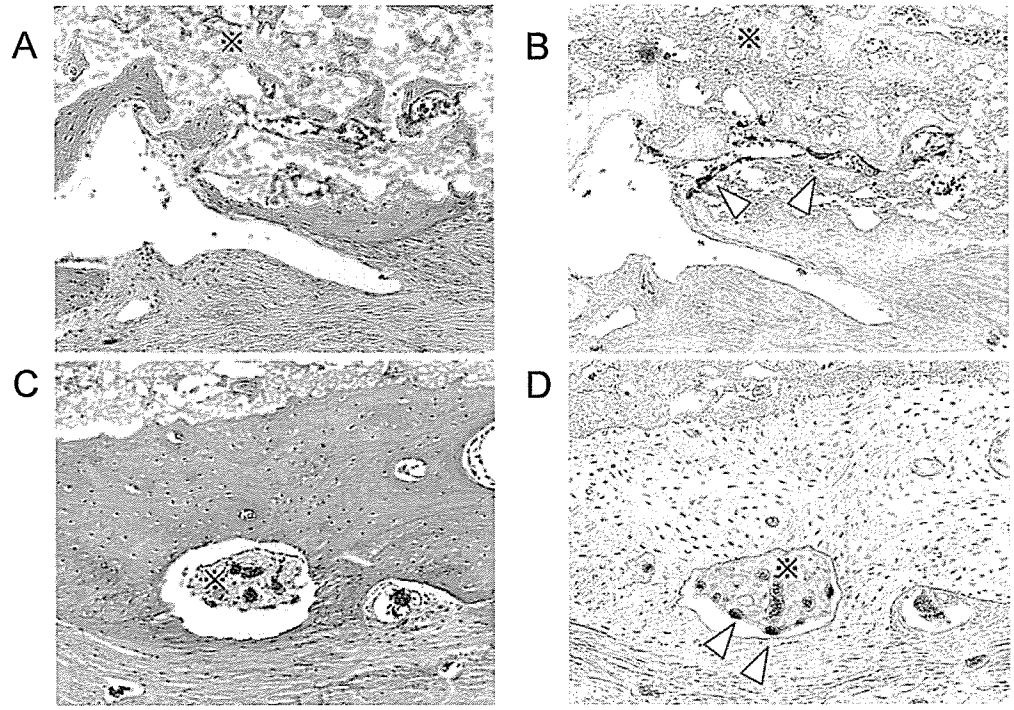

Fig. 7. Hematoxylin and eosin stain (**A** and **C**) and tartrate-resistant acid phosphatase stain (**B** and **D**) of serial sections of the tailor-made TCP implant. In the cylindrical holes, osteoclasts (*arrowheads*) were seen to resorb induced bone (**A** and **B**). In some areas of the TI, osteoclasts were seen to invade and probably resorb the implant. *Asterisk*, residual TI

as to designing internal structures that may facilitate bone regeneration. The TIs well matched the shape of the bone defect and therefore could be easily implanted to the defects during surgery. This matching of the shape helped to reduce the time for the operation and may have contributed to the good healing of the defects. The mechanical strength of the implant was sufficient for surgical handling and remained unbroken after surgery. In contrast, it was difficult and time-consuming to match the shape of HIs to the bone defects, because the sintering process turns the HI brittle.

Several researchers have explored the macropore size and interconnectivity of ceramic materials for osteoconductivity.[12,18] The optimal pore size for osteoconduction is 150–500μm in diameter. The properties of completely interconnected porous materials, very similar to the cancellous bone matrix, allow fibrovascular tissue to smoothly invade the deeper pore areas. In this study, we designed cylindrical holes 2mm in diameter running across the implants and found that bone formation on a larger scale was facilitated. The size of the micropores was also known to affect the performance of bone substitutes.[19] The size depends on the size of the powder particles and the properties of the binder agents. However, we could not dramatically vary these parameters because powder particles larger or smaller than 10μm caused defective distribution by the roller, and chondroitin sulfate at concentrations more or less than 5% caused clogging of the ink-head or blurring of the shape.

CT analysis revealed that the volume of the cylindrical holes decreased after the operation, and histological analysis revealed that newly formed bone tissue had invaded the cylindrical holes. In these holes, collagen tissue was first formed and subsequently bone tissue. Furthermore, bone marrow was also formed, suggesting that bone marrow formation does not necessarily occur after the replacement of artificial bone by newly forming bone. In the TIs, blood vessels invaded the body from the periphery and from inside the cylindrical holes. Together with the blood vessels, osteoclasts appeared and absorbed the implants. Thereafter, the invasion of collagen and bone tissues occurred mainly from the bone marrow. Usually, the replacement of trabecular bone, which is associated with bone marrow, is faster than that of cortical bone. Bone marrow formation in the TI may accelerate its replacement in the long run.

Bony bridge formation was observed in the TI-implanted group, but not in the HI-implanted group. The reason for this might be that the HI was manually cut and processed with lower precision than that of the TI; therefore, they did not match the shape of the defects and could easily separate from the bone stumps. Histologically, bone formation was clearly observed in the bridge formation part, whereas the surrounding area was covered by connective tissues. The HU level for the bridging bone was around 1000 HU, but it did not reach the HU level of cortical bone (around 1700).

Collectively, these data suggest that TIs fabricated by a 3D ink-jet printer facilitate bone healing. For clinical applications, acceleration of the replacement of TI by regenerated bone may be required.

Conclusion

The tailor-made TCP implants fabricated by a 3D ink-jet printer were safe and effective as a bone substitute. In the future, we plan to introduce bioactive agents using the ink-heads so that vascular invasion and bone regeneration is accelerated.

Acknowledgment We thank Hisayuki Sugiyama for kind assistance in working with the 3D software.

References

1. Tessier P, Kawamoto H, Matthews D, Posnick J, Raulo Y, Tulasne JF, Wolfe SA. Autogenous bone grafts and bone substitutes – tools and techniques: I. A 20000-case experience in maxillofacial and craniofacial surgery. Plast Reconstr Surg 2005;116(5 Suppl):6S–24S; discussion 92S–94S
2. Eppley BL, Pietrzak WS, Blanton MW. Allograft and alloplastic bone substitutes: a review of science and technology for the craniomaxillofacial surgeon. J Craniofac Surg 2005;16(6):981–989
3. Giannoudis PV, Dinopoulos H, Tsiridis E. Bone substitutes: an update. Injury 2005;36 Suppl 3:S20–S27
4. Mastrogiacomo M, Muraglia A, Komlev V, Peyrin F, Rustichelli F, Crovace A, Cancedda R. Tissue engineering of bone: search for a better scaffold. Orthod Craniofac Res 2005;8(4):277–284
5. Kenny SM, Buggy M. Bone cements and fillers: a review. J Mater Sci Mater Med 2003;14(11):923–938
6. Lalan S, Pomerantseva I, Vacanti JP. Tissue engineering and its potential impact on surgery. World J Surg 2001;25(11):1458–1466
7. Breitbart AS, Staffenberg DA, Thorne CH, Glat PM, Cunningham NS, Reddi AH, Ricci J, Steiner G. Tricalcium phosphate and osteogenin: a bioactive onlay bone graft substitute. Plast Reconstr Surg 1995;96(3):699–708
8. Rupprecht S, Merten HA, Kessler P, Wiltfang J. Hydroxyapatite cement (BoneSource) for repair of critical sized calvarian defects – an experimental study. J Craniomaxillofac Surg 2003;31(3): 149–153
9. Webb PA. A review of rapid prototyping (RP) techniques in the medical and biomedical sector. J Med Eng Technol 2000;24(4): 149–153
10. Lohfeld S, Barron V, McHugh PE. Biomodels of bone: a review. Ann Biomed Eng 2005;33(10):1295–1311
11. Curodeau A, Sachs E, Caldarise S. Design and fabrication of cast orthopedic implants with freeform surface textures from 3-D printed ceramic shell. J Biomed Mater Res 2000;53(5):525–535
12. Seitz H, Rieder W, Irsen S, Leukers B, Tille C. Three-dimensional printing of porous ceramic scaffolds for bone tissue engineering. J Biomed Mater Res B Appl Biomater 2005;74(2):782–788
13. Sun W, Darling A, Starly B, Nam J. Computer-aided tissue engineering: overview, scope and challenges. Biotechnol Appl Biochem 2004;39(Pt 1):29–47
14. Limpanuphap S, Derby B. Manufacture of biomaterials by a novel printing process. J Mater Sci Mater Med 2002;13(12):1163–1166
15. Lee M, Dunn JC, Wu BM. Scaffold fabrication by indirect three-dimensional printing. Biomaterials 2005;26(20):4281–4289
16. Hao H, Amizuka N, Oda K, Fujii N, Ohnishi H, Okada A, Nomura S, Maeda T. A histological evaluation on self-setting alpha-tricalcium phosphate applied in the rat bone cavity. Biomaterials 2004;25(3):431–442
17. Kokubo S, Mochizuki M, Fukushima S, Ito T, Nozaki K, Iwai T, Takahashi K, Yokota S, Miyata K, Sasaki N. Long-term stability of bone tissues induced by an osteoinductive biomaterial, recombinant human bone morphogenetic protein-2 and a biodegradable carrier. Biomaterials 2004;25(10):1795–1803
18. Hollister SJ, Lin CY, Saito E, Lin CY, Schek RD, Taboas JM, Williams JM, Partee B, Flanagan CL, Diggs A, Wilke EN, Van Lenthe GH, Muller R, Wirtz T, Das S, Feinberg SE, Krebsbach PH. Engineering craniofacial scaffolds. Orthod Craniofac Res 2005;8(3):162–173
19. Habibovic P, Sees TM, van den Doel MA, van Blitterswijk CA, de Groot K. Osteoinduction by biomaterials – physicochemical and structural influences. J Biomed Mater Res A 2006;77(4):747–762

ARTHRITIS & RHEUMATISM
Vol. 54, No. 8, August 2006, pp 2462–2470
DOI 10.1002/art.22041

Contribution of Runt-Related Transcription Factor 2 to the Pathogenesis of Osteoarthritis in Mice After Induction of Knee Joint Instability

Satoru Kamekura,[1] Yosuke Kawasaki,[1] Kazuto Hoshi,[1] Takashi Shimoaka,[1] Hirotaka Chikuda,[1] Zenjiro Maruyama,[1] Toshihisa Komori,[2] Shingo Sato,[3] Shu Takeda,[3] Gerard Karsenty,[4] Kozo Nakamura,[1] Ung-il Chung,[1] and Hiroshi Kawaguchi[1]

Objective. **By producing instability in mouse knee joints, we attempted to determine the involvement of runt-related transcription factor 2 (RUNX-2), which is required for chondrocyte hypertrophy, in the development of osteoarthritis (OA).**

Methods. **An experimental mouse OA model was created by surgical transection of the medial collateral ligament and resection of the medial meniscus of the knee joints of heterozygous RUNX-2–deficient ($Runx2^{+/-}$) mice and wild-type littermates. Cartilage destruction and osteophyte formation in the medial tibial cartilage were compared by histologic and radiographic analyses. Localization of type X collagen and matrix metalloproteinase 13 (MMP-13) was examined by immunohistochemistry. Localization of RUNX-2 was determined by X-Gal staining in heterozygous RUNX-2–deficient mice with the *lacZ* gene insertion at the *Runx2*-deletion site ($Runx2^{+/lacZ}$). Messenger RNA levels of type X collagen, MMP-13, and RUNX-2 were examined by real-time reverse transcriptase–polymerase chain reaction analysis.**

Results. **RUNX-2 was induced in the articular cartilage of wild-type mice at the early stage of OA, almost simultaneously with type X collagen but earlier than MMP-13. $Runx2^{+/-}$ and $Runx2^{+/lacZ}$ mice showed normal skeletal development and articular cartilage; however, after induction of knee joint instability, they exhibited decreased cartilage destruction and osteophyte formation, along with reduced type X collagen and MMP-13 expression, as compared with wild-type mice.**

Conclusion. **RUNX-2 contributes to the pathogenesis of OA through chondrocyte hypertrophy and matrix breakdown after the induction of joint instability.**

Osteoarthritis (OA), a chronic degenerative joint disorder characterized by articular cartilage destruction and osteophyte formation, is a major cause of disability in the elderly. Despite significant demand for more information, risk factors for this disease, as identified by epidemiologic studies, have to date been limited to age, obesity, trauma history, occupation, and sex (1,2). Since these factors are closely related to the accumulation of mechanical loading on joints, mechanical instability of the joints may play some role in OA pathogenesis. In an effort to clarify the mechanisms whereby joint instability leads to the development of OA, experimental animal models of OA induced by producing instability in the joints by surgical intervention have been developed in dogs, rabbits, guinea pigs, and rats (3–9). Due to recent progress in mouse genomics and the availability of transgenic and knockout mice, the mouse is currently the ideal animal for molecular study. Using a microsurgical technique to produce instability in the knee joints of mice, we established models of mechanical instability–induced OA that were reproducible and resembled OA in humans (10).

Supported by a Grant-in-Aid for Scientific Research from the Japanese Ministry of Education, Culture, Sports, Science, and Technology (15209049).

[1]Satoru Kamekura, MD, Yosuke Kawasaki, MD, Kazuto Hoshi, MD, Takashi Shimoaka, MD, Hirotaka Chikuda, MD, Zenjiro Maruyama, MD, Kozo Nakamura, MD, Ung-il Chung, MD, Hiroshi Kawaguchi, MD, PhD: Faculty of Medicine, University of Tokyo, Tokyo, Japan; [2]Toshihisa Komori, MD: Nagasaki University Graduate School of Biomedical Sciences, Nagasaki, Japan; [3]Shingo Sato, MD, Shu Takeda, MD: Tokyo Medical and Dental University, Tokyo, Japan; [4]Gerard Karsenty, MD: Baylor College of Medicine, Houston, Texas.

Address correspondence and reprint requests to Hiroshi Kawaguchi, MD, PhD, Sensory and Motor System Medicine, Faculty of Medicine, University of Tokyo, Hongo 7-3-1, Bunkyo, Tokyo 113-8655, Japan. E-mail: kawaguchi-ort@h.u-tokyo.ac.jp.

Submitted for publication November 24, 2005; accepted in revised form May 16, 2006.

We and other investigators (10–12) have previously reported that the early stage of OA is characterized by hypertrophic differentiation of chondrocytes, as determined by type X collagen expression in the superficial and middle zones of cartilage above the tidemark. Runt-related transcription factor 2 (RUNX-2), which was originally isolated on the basis of its ability to activate transcription of the osteoblast-specific osteocalcin gene (13,14), is known to be the only transcription factor that is required for chondrocyte hypertrophy (15–20). In the present study, therefore, we examined RUNX-2 expression in knee cartilage during OA progression, using our experimental mouse model. In addition, we investigated the functional involvement of RUNX-2 by comparing OA progression in heterozygous RUNX-2–deficient mice with that in wild-type mice.

MATERIALS AND METHODS

Animals. All experiments were performed according to the protocol approved by the Animal Care and Use Committee of the University of Tokyo. For the expression levels of type X collagen, matrix metalloproteinase 13 (MMP-13), type II collagen (CII), and RUNX-2 during OA progression, we used conventional wild-type C57BL/6 mice (8 weeks old) obtained from Charles River Japan (Yokohama, Japan). For the functional analyses of RUNX-2, we used heterozygous RUNX-2–deficient mice ($Runx2^{+/-}$) (129SVJ and C57BL/6 mixed background) that were created as previously reported (21), since homozygous RUNX-2–deficient ($Runx2^{-/-}$) mice died just after birth. $Runx2^{+/-}$ mice and the control wild-type littermates were generated by mating $Runx2^{+/-}$ mice. For the detection of RUNX-2 expression in situ, heterozygous RUNX-2–deficient mice with the *lacZ* gene inserted at the site of the *Runx2* gene deletion in 1 allele ($Runx2^{+/lacZ}$) (CBA and C57BL/6 mixed background) (22) were used (kindly provided by Dr. M. J. Owen, GlaxoSmithKline, London, UK). In total, we used 42 conventional mice, 42 $Runx2^{+/-}$ mice, 42 wild-type mice, and 24 $Runx2^{+/lacZ}$ mice.

OA model. The surgical procedure to create an experimental OA model was performed on 8-week-old mice as previously described (10). Briefly, under general anesthesia using pentobarbiturate (0.5 mg/10 gm body weight, intraperitoneally) (Sigma, St. Louis, MO), the bilateral hind limbs were prepared for aseptic surgery. The knee joint was exposed following a medial capsular incision and gentle lateral displacement of the extensor muscle, without transection of the patellar ligament. Then, the medial collateral ligament was transected, and the medial meniscus was removed using a surgical microscope and microsurgical technique. After replacement of the extensor muscle, the medial capsular incision was sutured, and the skin was closed. During the procedure, close attention was paid not to injure the articular cartilage. A sham operation was performed on the contralateral knee joint using the same approach, with no ligament transection or menisectomy. The animals were then allowed unrestricted activity, food, and water ad libitum.

Histologic analysis. At the indicated time points after surgery, the mice were killed, and the entire knee joints were dissected and fixed for 4 hours at 4°C in 4% paraformaldehyde buffered with phosphate buffered saline (PBS; pH 7.4). The specimens were decalcified for 2 weeks with 10% EDTA (pH 7.4) at 4°C. After the specimens were dehydrated with an increasing concentration of ethanol and embedded in paraffin, 4 μm of the frontal section was cut from the joints. Sections were stained with Safranin O–fast green. Development of OA was quantified by our original histologic grading scale of 0–4 for cartilage destruction (0 = no apparent changes, 1 = loss of superficial zone in articular catilage, 2 = defects limited to above tidemark, 3 = defects extending to calcified cartilage, and 4 = exposure of subchondral bone to cartilage destruction) and 0–3 for osteophyte formation (0 = none, 1 = formation of cartilage-like tissue [cartilaginous outgrowth], 2 = increase in cartilaginous matrix, and 3 = endochondral ossification or osteophyte formation), as previously described (10). The grades were scored as the most severe changes among >20 serial sections. A single observer (KH) who was blinded to the experimental group scored the sections.

Histomorphometric measurements of trabecular bone volume (bone volume/tissue volume) in the subchondral region of medial tibial joints were made according to the guidelines of the American Society of Bone and Mineral Research (23). Measurements of 2 separate sections per knee joint, spaced 50 μm apart, were obtained with an image analyzer (Histometry RT camera; System Supply, Nagano, Japan).

Immunohistochemistry. Immunohistochemical localization of type X collagen, MMP-13, and CII were performed in deparaffinized sections, as previously described (24). The sections were treated with 0.3% H_2O_2 in PBS for 30 minutes and with 2.5% hyaluronidase (Sigma) for 30 minutes. After blocking with 1% bovine serum albumin (Sigma) in PBS for 1 hour at room temperature, sections were incubated with polyclonal rabbit antibodies against rat type X collagen and CII (LSL, Tokyo, Japan), and polyclonal goat antibodies against rabbit MMP-13 (Chemicon, Temecula, CA) at a dilution of 1:100 for 24 hours at 4°C. As negative controls, we used nonimmune rabbit or goat IgG of the same dilution instead of the primary antibodies. The sections were rinsed in PBS and incubated for 20 minutes with Alexa Fluor 488–conjugated goat antibodies against rabbit IgG for type X collagen and with horseradish peroxidase–conjugated goat antibodies against rabbit IgG (ICN Biomedicals, Aurora, OH) for MMP-13 and CII. Visualization of immunoreactivity was performed using Alexa Fluor 488 fluorescence for type X collagen and by diaminobenzidine staining with methyl green counterstaining for MMP-13 and CII.

X-Gal staining. Since neither antibodies nor riboprobes worked appropriately in the localization of RUNX-2 by immunostaining or in situ hybridization of the cartilage tissue of adult mice, respectively, we used X-Gal staining to examine LacZ expression under control of RUNX-2 promoter activation in $Runx2^{+/lacZ}$ mice. Eight-week-old male $Runx2^{+/lacZ}$ mice that underwent the microsurgery described above were killed at 2, 4, and 8 weeks, and the entire knee joint was dissected. The specimens were fixed in 2% paraformaldehyde buffered with PBS (pH 7.4) for 1 hour at 4°C. To detect β-galactosidase activity, the tissues were stained with X-Gal, as previously described (22). The specimens were decalcified for

2 weeks with 10% EDTA (pH 7.4) at 4°C. After dehydration with an increasing concentration of ethanol and embedding in paraffin, 4 μm of the frontal section was cut from the joints.

Real-time reverse transcriptase–polymerase chain reaction (RT-PCR) analysis. To determine the messenger RNA (mRNA) levels of RUNX-2, type X collagen, and MMP-13 in OA cartilage, we collected the medial tibial cartilage from OA and sham-operated knee joints 2, 4, and 8 weeks after surgery, as previously described (25). Total RNA was extracted from the samples using the chaotropic TRIzol method, followed by isogen–chloroform extraction and isopropanol precipitation (Nippon Gene, Tokyo, Japan), according to the manufacturer's instructions. Total mRNA (1 μg) was reverse transcribed using Superscript reverse transcriptase with random hexamer (Takara Shuzo, Shiga, Japan), and 1 μl of each reverse transcriptase reaction was used as a template for the second-step SYBR Green real-time RT-PCR. The full-length or partial-length complementary DNA of target genes, including PCR amplicon sequences, was amplified by PCR, cloned into pCR-TOPO Zero II or pCR-TOPO II vectors (Invitrogen, Carlsbad, CA), and used as standard templates after linearization. QuantiTect SYBR Green PCR Master Mix (Qiagen, Chatsworth, CA) was used for the second-step SYBR Green real-time RT-PCR according to the manufacturer's instructions. SYBR Green PCR amplification and real-time fluorescence detection were performed using an ABI Prism 7700 sequence detection system (Applied Biosystems, Foster City, CA). All reactions were run in quadruplicate. Copy numbers of target gene mRNA in each total RNA were calculated by reference to standard curves and were adjusted to the mouse standard total RNA (ABI) with the mouse actin as an internal control. PCR amplification was performed using the following gene-specific primer pairs: for type X collagen, sense 5′-CATAAAGGGCCCACTTGCTA-3′ and antisense 5′-TGGCTGATATTCCTGGTGGT-3′; for MMP-13, sense 5′-AGGCCTTCAGAAAAGCCTTC-3′ and antisense 5′-TCCTTGGAGTGATCCAGACC-3′; for RUNX-2, sense 5′-CCCAGCCACCTTTACCTACA-3′ and antisense 5′-TATGGAGTGCTGCTGGTCTG-3′; and for actin, sense 5′-AGATGTGGATCAGCAAGCAG-3′ and antisense 5′-GCGCAAGTTAGGTTTTGTCA-3′. Data were normalized by the average mRNA level before the operation (time 0), and expressed as the mean ± SEM in 8–10 mice per group per time point.

Radiographic analysis. Radiographs of the knee joints of wild-type and $Runx2^{+/-}$ mice were obtained 12 weeks after surgery under general anesthesia using a soft x-ray apparatus (CMB-2; Softex, Tokyo, Japan).

Statistical analysis. Group means were compared by analysis of variance, and significance of differences was determined by post hoc testing with Bonferroni adjustment. *P* values less than 0.05 were considered significant.

RESULTS

Time course of type X collagen, MMP-13, and CII expression in OA cartilage. Among the 4 types of experimental mouse OA models, we used the medial model in this study, with transection of the medial collateral ligament and resection of the medial meniscus of the knee of 8-week-old male mice (10). This model exhibits the disorder in the medial portion, resembling the area most affected by OA in humans, and is suitable for observation of the early stage of OA, since it displays a relatively slow progression of the condition. In fact, Safranin O staining showed matrix degradation at 4 weeks after surgery and cartilage destruction into the middle zone at 8 weeks (Figure 1A).

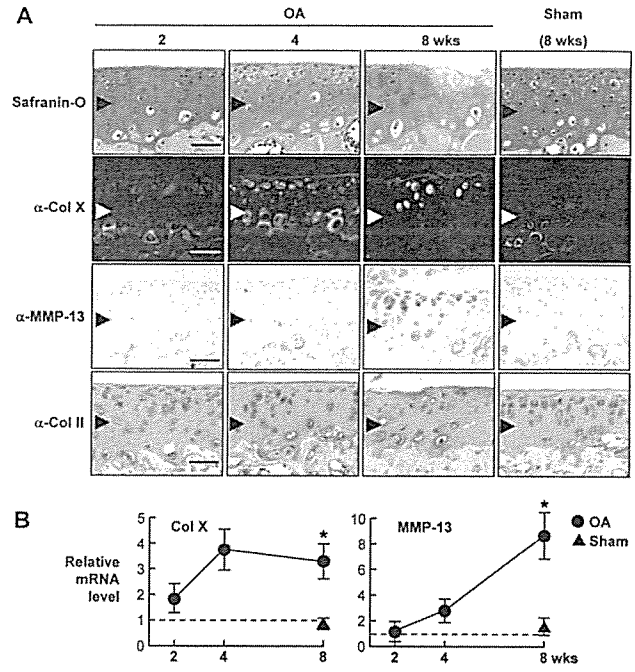

Figure 1. Time course of expression of type X collagen (Col X), matrix metalloproteinase 13 (MMP-13), and type II collagen (CII) in the medial portion of tibial cartilage during the development of osteoarthritis (OA) by induction of joint instability. Eight-week-old male wild-type mice underwent medial collateral ligament transection and medial meniscus resection in the right knee joint, as described in Materials and Methods. A sham operation was performed on the left knee joint, using the same approach. **A,** Representative histologic features of frontal sections of the right knee 2, 4, and 8 weeks after surgery and of the left knee 8 weeks after surgery. Safranin O staining and immunohistochemical staining with type X collagen, MMP-13, and CII antibodies were performed. Immunoreactivity was visualized with Alexa Fluor 488 fluorescence for type X collagen, and with diaminobenzidine staining with methyl green counterstaining for MMP-13 and CII. **Arrowheads** indicate the levels of the tidemark. Bars = 100 μm. **B,** Type X collagen and MMP-13 mRNA levels in medial tibial cartilage extracts from OA and sham-operated knee joints, determined by real-time reverse transcriptase–polymerase chain reaction analysis. Data were normalized to the average mRNA level before the operation (time 0) (set at 1) and are expressed as the mean ± SEM of 8 samples per group per time. * = $P < 0.01$ versus sham-operated knees.

Immunohistochemical analyses were performed

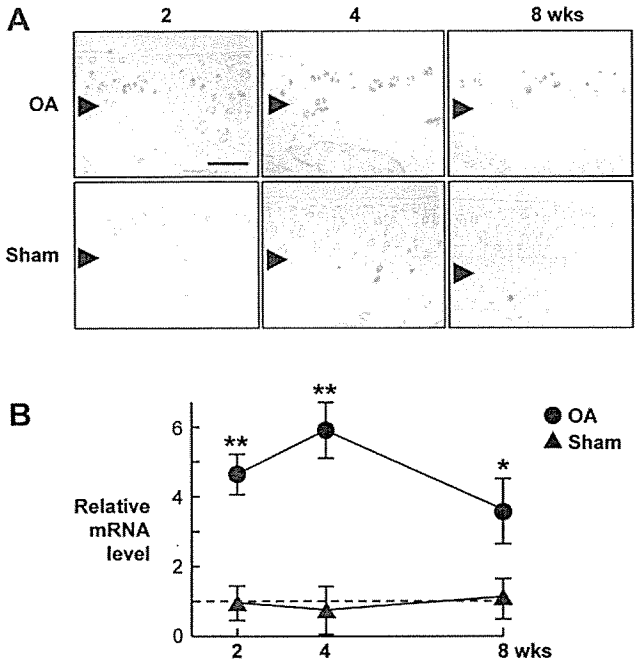

Figure 2. Time course of runt-related transcription factor 2 (RUNX-2) expression in the medial portion of tibial cartilage during development of osteoarthritis (OA) by induction of joint instability. **A,** Representative histologic features of frontal sections 2, 4, and 8 weeks after surgery. For runt-related transcription factor 2 (RUNX-2) expression in situ, 8-week-old male $Runx2^{+/lacZ}$ mice (n = 4 per group per time) underwent microsurgery or sham operation as described in Materials and Methods, and the specimens were stained with X-Gal to detect β-galactosidase activity. **Arrowheads** indicate the level of the tidemark. Bar = 100 μm. **B,** RUNX-2 mRNA level in medial tibial cartilage extracts from OA and sham-operated knee joints of conventional wild-type mice, as determined by real-time reverse transcriptase–polymerase chain reaction analysis. Data were normalized to the average mRNA level before the operation (time 0) (set at 1) and are expressed as the mean ± SEM of 8 samples per group per time. * = $P < 0.05$; ** = $P < 0.01$ versus sham-operated knees.

in this model to assess the time course of type X collagen and MMP-13 expression, which in our previous study (10), were shown to be most strongly induced among collagens and MMPs during OA progression. Although type X collagen expression was limited to the deep calcified zone below the tidemark in the sham-operated knee and at 2 weeks after OA induction, at 4 weeks, it appeared in the superficial and middle zones above the tidemark. MMP-13 expression was not detected above the tidemark at 2 or 4 weeks; however, it was clearly localized in hypertrophic chondrocytes at 8 weeks. The up-regulation of type X collagen and MMP-13 occurred only in the medial portion of the knee joint, where the mechanical instability was loaded, but not in the unaffected lateral portion (data not shown). In contrast, the immunolocalization of CII was unaltered during OA progression, as we previously reported (10). Quantification of mRNA levels in cartilage extracts by real-time RT-PCR analysis confirmed the distinct time course of the expression of type X collagen and MMP-13 (Figure 1B). These findings suggest that articular chondrocytes undergo hypertrophic differentiation in response to joint instability at an early stage, and the hypertrophic chondrocytes express MMP-13, which may degrade the cartilage matrix.

Time course of RUNX-2 expression in OA cartilage. We examined the involvement of RUNX-2, a transcriptional activator that has been known to induce both chondrocyte hypertrophy and MMP-13 expression (15–20,26,27). We initially created the medial OA model in the knee joint of $Runx2^{+/lacZ}$ mice, and examined RUNX-2 expression by X-Gal staining. Time course analysis of the sham-operated cartilage revealed that RUNX-2 expression was positive in some chondrocytes in calcified cartilage below the tidemark, but was not visible in cells above the tidemark (Figure 2A). In contrast, RUNX-2 expression was induced above the tidemark in the OA cartilage as early as 2 weeks, was enhanced at 4 weeks, and decreased thereafter until 8 weeks. This RUNX-2 induction also occurred only in the medial portion of the joint, where the mechanical instability was loaded, but not in the unaffected lateral portion (data not shown). Real-time RT-PCR analysis of cartilage extracts from conventional wild-type mice confirmed the time course of the RUNX-2 mRNA level during OA progression (Figure 2B), suggesting the involvement of RUNX-2 in the early stage of OA.

Effects of RUNX-2 insufficiency on type X collagen and MMP-13 expression in OA cartilage. To determine the involvement of RUNX-2 in the induction of type X collagen and MMP-13 during OA progression, we examined the expression in $Runx2^{+/-}$ mice. The $Runx2^{+/-}$ mice, as well as $Runx2^{+/lacZ}$ mice, showed normal skeletal development and articular cartilage under physiologic conditions (data not shown). We therefore created the medial OA model in 8-week-old mice and compared the expression of type X collagen and MMP-13 in the medial tibial cartilage during OA progression. We first confirmed, by real-time RT-PCR analysis, that RUNX-2 mRNA levels were increased at 4 and 8 weeks after surgery in wild-type mice, while levels at both times were significantly reduced to less than half in $Runx2^{+/-}$ mice (Figure 3B). Immunohistochemical analysis showed that type X collagen expression was visible above the tidemark in the articular cartilage of wild-type mice at 4 and 8 weeks after surgery; however,

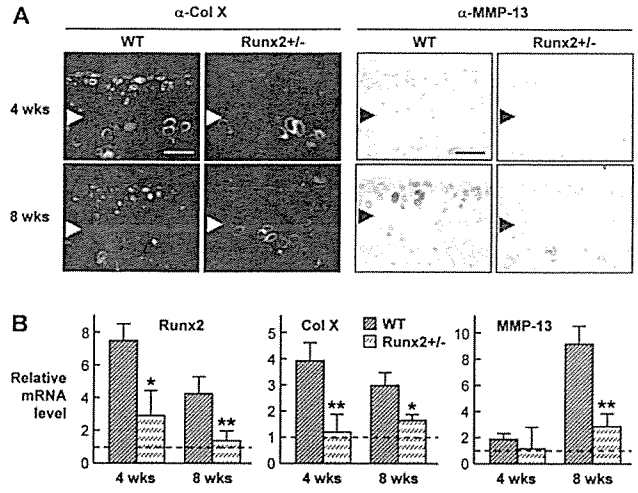

Figure 3. Type X collagen, MMP-13, and RUNX-2 expression in the medial portion of tibial cartilage of wild-type (WT) and Runx2$^{+/-}$ mice during development of OA by induction of joint instability. Eight-week-old male wild-type and Runx2$^{+/-}$ mice underwent microsurgery to induce OA in the knee joints. Samples were prepared and stained as described in Figure 1. **A,** Representative immunohistochemical staining of frontal sections 4 and 8 weeks after surgery. **Arrowheads** indicate the level of the tidemark. Bars = 100 μm. **B,** RUNX-2, type X collagen, and MMP-13 mRNA levels in medial tibial cartilage extracts from wild-type and Runx2$^{+/-}$ mice, determined by real-time reverse transcriptase–polymerase chain reaction analysis. Data were normalized to the average mRNA level before the operation (time 0) (set at 1) and are expressed as the mean and SEM of 8 samples per group per time. * = $P < 0.05$; ** = $P < 0.01$ versus wild-type mice. See Figure 1 for other definitions.

this was rarely seen in the articular cartilage of Runx2$^{+/-}$ mice, except in the calcified cartilage below the tidemark (Figure 3A). MMP-13 expression was also increased above the tidemark in the articular cartilage of wild-type mice at 8 weeks, which was significantly reduced in the cartilage of Runx2$^{+/-}$ mice. Real-time RT-PCR analysis confirmed that both type X collagen and MMP-13 mRNA levels were decreased by RUNX-2 insufficiency (Figure 3B), indicating that chondrocyte hypertrophy and MMP-13 induction during OA progression are at least partly mediated by RUNX-2.

Effect of RUNX-2 insufficiency on OA progression. To further investigate the contribution of RUNX-2 to the development of OA, we next compared the susceptibility of cartilage destruction and osteophyte formation between joints from wild-type and Runx2$^{+/-}$ mice, using joint instability in the medial model. Safranin O staining of cartilage in wild-type mice showed that cartilage destruction progressed into the middle zone by 8 weeks after surgery and reached the calcified cartilage layer across the tidemark by 12 weeks (Figure 4A). The cartilage destruction in Runx2$^{+/-}$ mice was much milder, however, and it was confined within the middle zone throughout the observation period. The Runx2$^{+/lacZ}$ joint was confirmed to exhibit cartilage destruction similar to that of Runx2$^{+/-}$ mice and milder than wild-type mice. Quantification by our original grading system (10) revealed significant reduction of cartilage destruction by the RUNX-2 insufficiency at 8 weeks and thereafter (Figure 4B).

Osteophyte formation, the other characteristic feature of OA, was detected at the medial edge of the joints of wild-type mice 12 weeks after surgery in both radiographic (Figure 5A) and histologic (Figure 5B) analyses. Joints in the Runx2$^{+/-}$ and Runx2$^{+/lacZ}$ mice showed decreased cartilaginous outgrowth and osteo-

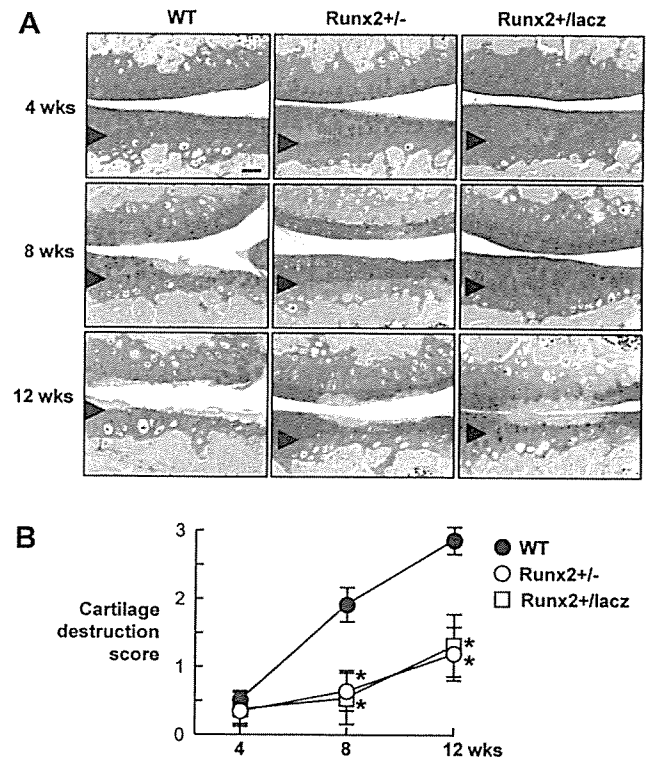

Figure 4. Time course of cartilage destruction in the medial portion of tibial cartilage of wild-type (WT), Runx2$^{+/-}$, and Runx2$^{+/lacZ}$ mice after induction of joint instability. Eight-week-old male mice underwent microsurgery to induce osteoarthritis in the knee joints, and the samples were prepared and stained. **A,** Representative histologic features (Safranin O staining) of frontal sections 4, 8, and 12 weeks after surgery. **Arrowheads** indicate the level of the tidemark. Bar = 100 μm. **B,** Histologic scoring of cartilage destruction according to the grading system described in Materials and Methods. Data are expressed as the mean ± SEM of 10 samples per genotype per time for wild-type and Runx2$^{+/-}$ mice, and of 4 samples per time for Runx2$^{+/LacZ}$ mice. * = $P < 0.01$ versus wild-type mice.

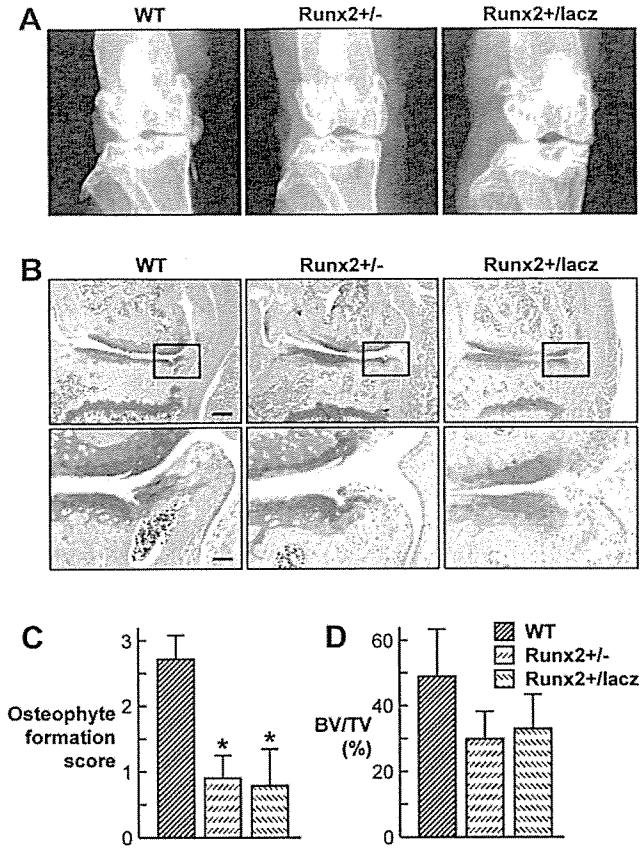

Figure 5. Osteophyte formation in the medial portion of tibial cartilage of wild-type (WT), $Runx2^{+/-}$, and $Runx2^{+/lacZ}$ mice 12 weeks after induction of joint instability. **A,** Representative anteroposterior radiographs. **B,** Representative histologic features of frontal sections (Safranin O staining). Boxed areas in the top row indicate the regions shown at higher magnification in the bottom row. Bars = 200 μm (top) and 50 μm (bottom). **C,** Histologic scoring of osteophyte formation according to the grading system described in Materials and Methods. **D,** Histomorphometric measurements of trabecular bone volume (bone volume/tissue volume [BV/TV]) in the subchondral region of medial tibial joints. Data in **C** and **D** are expressed as the mean and SEM of 10 samples per genotype per time for wild-type and $Runx2^{+/-}$ mice, and of 4 samples per time for $Runx2^{+/LacZ}$ mice. * = $P < 0.01$ versus wild-type mice.

phyte formation. Quantification by the osteophyte formation score (10) at 12 weeks confirmed the reduction by RUNX-2 insufficiency (Figure 5C). The trabecular bone volume in the subchondral region tended to be lower in mice with RUNX-2 insufficiency, although not statistically significant (Figure 5D). These findings demonstrate that RUNX-2 contributes to at least 2 characteristic features of OA: cartilage destruction and osteophyte formation under the unstable joint.

DISCUSSION

Although several studies have examined the expression of matrix proteins in OA cartilage using experimental models in larger animals, such as dogs and rabbits (3–7,9), the results have been inconsistent. For example, in rabbit models 1 study showed no alteration of CII expression (7), while another showed its up-regulation at region-specific sites (5). In canine models, CII expression was higher in OA knee joints, and expression progressed in one study (4) and decreased in another one (6). Other matrix proteins, such as aggrecan and fibromodulin, seem to be altered only at isolated time points (5,7).

Our previous immunohistochemical analyses using an experimental mouse OA model (medial model) showed no substantial change in CII, type IX collagen, MMP-2, MMP-3, or MMP-9 expression, but up-regulation of type X collagen and MMP-13 (10). The present time course analyses using the same model confirmed up-regulation of type X collagen and MMP-13 with no alteration of CII, by immunohistochemical and real-time RT-PCR analyses. In this model, definite increases in RUNX-2, type X collagen, and MMP-13 were seen at 2, 4, and 8 weeks, respectively, after surgery (Figures 1 and 2), while cartilage destruction became visible at 8 weeks (10). In addition, RUNX-2 insufficiency caused a decrease in cartilage destruction, along with a reduction in type X collagen and MMP-13 expression. Furthermore, transgenic mice expressing constitutively active MMP-13 are reported to exhibit articular cartilage destruction resembling OA (28). These findings indicate that induction of these molecules is the cause, not the effect, of the cartilage destruction.

Under physiologic conditions, articular cartilage does not show chondrocyte hypertrophy, but maintains the stable phenotype as a permanent cartilage. However, in OA articular cartilage, pathologic expression of type X collagen and other differentiation markers, including annexin VI, alkaline phosphatase, osteopontin, and osteocalcin, have been reported (11,12,29–31), indicating that OA articular cartilage cannot maintain the characteristics of the permanent cartilage, but gains those of the growth plate cartilage, which undergoes endochondral ossification. MMP-13, which potently degrades cartilage matrix with a preference for CII, is known to be induced in OA articular cartilage (32) and to be functionally involved in OA pathogenesis (28). This proteinase has been suggested to be induced in response to proinflammatory cytokines such as tumor necrosis factor

α (TNFα), interleukin-1 (IL-1), and IL-6 in articular cartilage under pathologic conditions, such as OA and rheumatoid arthritis (RA) (2,33). However, it is suspicious that these cytokines play significant roles in the development of OA. Our previous study showed that levels of TNFα, IL-1, IL-6, as well as fibroblast growth factor 2, in the synovial fluid from knee joints of patients with OA were much lower than those from patients with RA (34).

Furthermore, a recent study using a mouse OA model similar to ours (35) showed that mice lacking IL-1, IL-1β–converting enzyme, stromelysin 1, or inducible nitric oxide synthase unexpectedly exhibited an acceleration of cartilage destruction, implying that these proinflammatory factors do not stimulate, but rather inhibit, cartilage destruction. Instead, we propose that chondrocyte hypertrophy is important for MMP-13 induction in cartilage. There are well-ordered expression patterns of type X collagen and MMP-13 in the growth plate cartilage; only the highly differentiated cells in the type X collagen–positive hypertrophic chondrocytes are able to express MMP-13 (10,36,37). This sequence of expression may be essential for endochondral ossification that needs prior degradation of the cartilage matrix. The present time-course study also showed that MMP-13 expression occurred later than hypertrophic differentiation of OA chondrocytes, suggesting the principal role of chondrocyte hypertrophy in the development of OA.

Although several signaling molecules, including Indian hedgehog and parathyroid hormone–related peptide, have been shown in mouse genetics studies to regulate chondrocyte hypertrophy, RUNX-2 is known to be the only transcription factor that is necessary for hypertrophy, based on several lines of evidence. $Runx2^{-/-}$ mice show no hypertrophic chondrocytes in some skeletal elements (15,16), and expression of a dominant-negative *Runx2* mutation inhibits chondrocyte hypertrophy and ossification in vivo (18). Constitutive expression of RUNX-2 in prehypertrophic chondrocytes leads to premature and ectopic chondrocyte hypertrophy (17–19). In addition, endogenous RUNX-2 is known to be expressed mainly in prehypertrophic chondrocytes during endochondral ossification in skeletal development and growth (15,19). The present analysis also showed that RUNX-2 expression reached a maximum at 2–4 weeks and decreased at 8 weeks, suggesting that RUNX-2 is expressed in prehypertrophic chondrocytes that undergo hypertrophic differentiation and apoptosis thereafter in the OA cartilage as well.

The fact that type X collagen was induced shortly after RUNX-2 during OA progression is consistent with a recent finding that type X collagen is a direct transcriptional target of RUNX-2 by transactivation of the promoter (20). However, the time lag between RUNX-2 and MMP-13 expression was inconsistent with previous reports showing the direct activation of MMP-13 transcription by RUNX-2 (26,27). RUNX-2 may therefore induce type X collagen expression directly, and then the hypertrophic chondrocytes express MMP-13 during the development of OA.

The mechanism whereby mechanical instability induces RUNX-2 expression in articular cartilage remains unclarified. RUNX-2 was recently reported to be a target of mechanical signals, mainly in osteoblasts, causing anabolic action in bone. Low-level stretching, as well as extracellular nucleotides released in response to mechanical stimuli, up-regulates not only RUNX-2 expression, but also its DNA binding activity in cultured osteoblasts (38,39). This effect in bone was shown to be modulated by activation of ERK MAPK and protein kinase C.

In contrast, more complicated mechanoresponsive mechanisms appear to evolve in chondrocytes. Although tensile strain increased RUNX-2 expression, hydrostatic pressure decreased it somewhat in cultured primary chondrocytes (40). In fact, our preliminary experiment using the culture of chondrocytes isolated from the growth plate of wild-type and $Runx2^{+/-}$ mice, as described previously (41), failed to show induction of RUNX-2 by stretching stimulation using the Flexercell culture system (data not shown). Since we also could not find RUNX-2 induction in OA superficial chondrocytes earlier than 2 weeks after surgery (data not shown), it is likely that the induction is not directly from mechanical instability, but occurs by way of changes in other molecules. Establishment of a chondrocyte culture system that accurately reproduces the in vivo environment of OA articular cartilage induced by joint instability will be essential to elucidate the molecular network mediating RUNX-2 expression.

Accumulation of mechanical loading and the subsequent cartilage destruction were confined to the medial portion of the tibial cartilage in the present model, and the changes in RUNX-2, type X collagen, and MMP-13 were detected mainly in the affected medial portion. However, a previous study (9) has shown that expression levels of CII, type I collagen, and YKL-40 were up-regulated independently of joint localization during the early stages in an experimental canine OA model (3). Another study of expression levels of CII, aggrecan, biglycan, decorin, fibromodulin, and MMPs 1,

3, and 13 demonstrated significant region-specific changes in a rabbit OA model (5). Although the present study failed to detect the up-regulation of RUNX-2, type X collagen, or MMP-13 in the unaffected lateral portion, further studies of region-specific expression of a subset of transcription factors, cytokines, matrix molecules, proteinases, and proteinase inhibitors should elucidate the molecular network underlying the OA pathogenesis in the whole joint.

Although OA has long been considered to be primarily a cartilage disorder associated with focal articular cartilage degradation, recent studies suggest the involvement of subchondral trabecular bone in the pathophysiology (8,42,43). The increased subchondral bone stiffness is suggested to reduce the ability to dissipate the load and distribute the strain generated within the joint, which augments peak dynamic forces in the overlying articular cartilage and can accelerate its damage over time. In fact, the present study showed a decrease in the subchondral trabecular bone volume in mice with RUNX-2 insufficiency, although it was not statistically significant. Considering that *Runx2* is originally known as a master gene for bone formation, we cannot deny the possibility that reduced cartilage destruction due to RUNX-2 insufficiency is at least partly secondary to the decreased subchondral bone. Further analyses using bone- and cartilage-specific RUNX-2–deficient mice driven by type I collagen and CII promoters, respectively, would determine the tissue-specific role of RUNX-2 during OA progression.

We herein propose a mechanism of OA development, in which RUNX-2 expression induced by mechanical instability causes pathologic hypertrophic differentiation of articular chondrocytes, which then produces MMP-13 that degrades cartilage matrix. We certainly do not think that MMP-13 is the sole proteinase for cartilage degradation in OA. In fact, deletion of active ADAMTS-5 (aggrecanase 2), another member of the metalloproteinase family, was recently reported to prevent cartilage destruction in mouse arthritis models (44,45). We speculate that the cartilage degradation by these metalloproteinases may lead to osteophyte formation through endochondral ossification at the edge of the articular cartilage to which new blood vessels are accessible by adjacent synovial or fibrous tissue. But it may result in cartilage destruction without ossification at the avascular central area.

The fact that RUNX-2 insufficiency prevented both cartilage destruction and osteophyte formation without affecting physiologic skeletal conditions suggests that this molecule can clinically be a therapeutic target of these disorders, since RUNX-2 is known to be induced in human OA cartilage (46). Mutations in the *Runx2* gene cause cleidocranial dysplasia not only in mice, but also in humans (22,47,48). Although various types of the human *RUNX-2* gene, including chromosomal translocations, deletions, insertions, nonsense, missense, and splice-site mutations, have been reported to cause a wide spectrum of phenotypic variability, ranging from primary dental anomalies to all typical features plus osteoporosis, future studies on the susceptibility of OA in these patients will provide invaluable information on the possibility that RUNX-2 is a clinical target for this common joint disorder.

ACKNOWLEDGMENTS

We thank Dr. Michael Owen for providing the $Runx2^{+/lacZ}$ mice. We also thank Reiko Yamaguchi, Mizue Ikeuchi, Shinpei Sotoyama, and Motoki Miyazawa for their excellent technical assistance.

REFERENCES

1. Doherty M. Risk factors for progression of knee osteoarthritis. Lancet 2001;358:775–6.
2. Poole AR, Howell DS. Etiopathies of osteoarthritis. In: Moskowitz RW, Howell DS, Altman RD, Buckwalter JA, Goldberg VM, editors. Osteoarthritis: Diagnosis and medical/surgical management. 3rd ed. Philadelphia: Saunders; 2001. p. 29–47.
3. Pond MJ, Nuki G. Experimentally-induced osteoarthritis in the dog. Ann Rheum Dis 1973;32:387–8.
4. Matyas JR, Ehlers PF, Huang D, Adams ME. The early molecular natural history of experimental osteoarthritis. I. Progressive discoordinate expression of aggrecan and type II procollagen messenger RNA in the articular cartilage of adult animals. Arthritis Rheum 1999;42:993–1002.
5. Le Graverand MP, Eggerer J, Vignon E, Otterness IG, Barclay L, Hart DA. Assessment of specific mRNA levels in cartilage regions in a lapine model of osteoarthritis. J Orthop Res 2002;20:535–44.
6. Matyas JR, Huang D, Chung M, Adams ME. Regional quantification of cartilage type II collagen and aggrecan messenger RNA in joints with early experimental osteoarthritis. Arthritis Rheum 2002;46:1536–43.
7. Bluteau G, Gouttenoire J, Conrozier T, Mathieu P, Vignon E, Richard M, et al. Differential gene expression analysis in a rabbit model of osteoarthritis induced by anterior cruciate ligament (ACL) section. Biorheology 2002;39:247–58.
8. Hayami T, Pickarski M, Wesolowski GA, McLane J, Bone A, Destefano J, et al. The role of subchondral bone remodeling in osteoarthritis: reduction of cartilage degeneration and prevention of osteophyte formation by alendronate in the rat anterior cruciate ligament transection model. Arthritis Rheum 2004;50:1193–206.
9. Lorenz H, Wenz W, Ivancic M, Steck E, Richter W. Early and stable upregulation of collagen type II, collagen type I and YKL40 expression levels in cartilage during early experimental osteoarthritis occurs independent of joint location and histological grading. Arthritis Res Ther 2005;7:R156–65.
10. Kamekura S, Hoshi K, Shimoaka T, Chung U, Chikuda H, Yamada T, et al. Osteoarthritis development in novel experimental mouse models induced by knee joint instability. Osteoarthritis Cartilage 2005;13:632–41.

11. Von der Mark K, Kirsch T, Nerlich A, Kuss A, Weseloh G, Gluckert K, et al. Type X collagen synthesis in human osteoarthritic cartilage: indication of chondrocyte hypertrophy. Arthritis Rheum 1992;35:806–11.
12. Boos N, Nerlich AG, Wiest I, von der Mark K, Ganz R, Aebi M. Immunohistochemical analysis of type-X-collagen expression in osteoarthritis of the hip joint. J Orthop Res 1999;17:495–502.
13. Ducy P, Zhang R, Geoffroy V, Ridall AL, Karsenty G. Osf2/Cbfa1: a transcriptional activator of osteoblast differentiation. Cell 1997;89:747–54.
14. Karsenty G, Wagner EF. Reaching a genetic and molecular understanding of skeletal development [review]. Dev Cell 2002;2:389–406.
15. Inada M, Yasui T, Nomura S, Miyake S, Deguchi K, Himeno M, et al. Maturational disturbance of chondrocytes in Cbfa1-deficient mice. Dev Dyn 1999;214:279–90.
16. Kim IS, Otto F, Zabel B, Mundlos S. Regulation of chondrocyte differentiation by Cbfa1. Mech Dev 1999;80:159–70.
17. Enomoto H, Enomoto-Iwamoto M, Iwamoto M, Nomura S, Himeno M, Kitamura Y, et al. Cbfa1 is a positive regulatory factor in chondrocyte maturation. J Biol Chem 2000;275:8695–702.
18. Ueta C, Iwamoto M, Kanatani N, Yoshida C, Liu Y, Enomoto-Iwamoto M, et al. Skeletal malformations caused by overexpression of Cbfa1 or its dominant negative form in chondrocytes. J Cell Biol 2001;153:87–100.
19. Takeda S, Bonnamy JP, Owen MJ, Ducy P, Karsenty G. Continuous expression of Cbfa1 in nonhypertrophic chondrocytes uncovers its ability to induce hypertrophic chondrocyte differentiation and partially rescues Cbfa1-deficient mice. Genes Dev 2001;15:467–81.
20. Zheng Q, Zhou G, Morello R, Chen Y, Garcia-Rojas X, Lee B. Type X collagen gene regulation by Runx2 contributes directly to its hypertrophic chondrocyte-specific expression in vivo. J Cell Biol 2003;162:833–42.
21. Komori T, Yagi H, Nomura S, Yamaguchi A, Sasaki K, Deguchi K, et al. Targeted disruption of Cbfa1 results in a complete lack of bone formation owing to maturational arrest of osteoblasts. Cell 1997;89:755–64.
22. Otto F, Thornell AP, Crompton T, Denzel A, Gilmour KC, Rosewell IR, et al. Cbfa1, a candidate gene for cleidocranial dysplasia syndrome, is essential for osteoblast differentiation and bone development. Cell 1997;89:765–71.
23. Parfitt AM, Drezner MK, Glorieux FH, Kanis JA, Malluche H, Meunier PJ, et al. Bone histomorphometry: standardization of nomenclature, symbols, and units. J Bone Miner Res 1987;2:595–610.
24. Hoshi K, Komori T, Ozawa H. Morphological characterization of skeletal cells in Cbfa1-deficient mice. Bone 1999;25:639–51.
25. Xu L, Peng H, Wu D, Hu K, Goldring MB, Olsen BR, et al. Activation of the discoidin domain receptor 2 induces expression of matrix metalloproteinase 13 associated with osteoarthritis in mice. J Biol Chem 2005;280:548–55.
26. Jimenez MJ, Balbin M, Lopez JM, Alvarez J, Komori T, Lopez-Otin C. Collagenase 3 is a target of Cbfa1, a transcription factor of the runt gene family involved in bone formation. Mol Cell Biol 1999;19:4431–42.
27. Porte D, Tuckermann J, Becker M, Baumann B, Teurich S, Higgins T, et al. Both AP-1 and Cbfa1-like factors are required for the induction of interstitial collagenase by parathyroid hormone. Oncogene 1999;18:667–78.
28. Neuhold LA, Killar L, Zhao W, Sung ML, Warner L, Kulik J, et al. Postnatal expression in hyaline cartilage of constitutively active human collagenase-3 (MMP-13) induces osteoarthritis in mice. J Clin Invest 2001;107:35–44.
29. Pullig O, Weseloh G, Gauer S, Swoboda B. Osteopontin is expressed by adult human osteoarthritic chondrocytes: protein and mRNA analysis of normal and osteoarthritic cartilage. Matrix Biol 2000;19:245–55.
30. Pullig O, Weseloh G, Ronneberger D, Kakonen S, Swoboda B. Chondrocyte differentiation in human osteoarthritis: expression of osteocalcin in normal and osteoarthritic cartilage and bone. Calcif Tissue Int 2000;67:230–40.
31. Pfander D, Swoboda B, Kirsch T. Expression of early and late differentiation markers (proliferating cell nuclear antigen, syndecan-3, annexin VI, and alkaline phosphatase) by human osteoarthritic chondrocytes. Am J Pathol 2001;159:1777–83.
32. Billinghurst RC, Dahlberg L, Ionescu M, Reiner A, Bourne R, Rorabeck C, et al. Enhanced cleavage of type II collagen by collagenases in osteoarthritic articular cartilage. J Clin Invest 1997;99:1534–45.
33. Vincenti MP, Brinckerhoff CE. Transcriptional regulation of collagenase (MMP-1, MMP-13) genes in arthritis: integration of complex signaling pathways for the recruitment of gene-specific transcription factors [review]. Arthritis Res 2002;4:157–64.
34. Manabe N, Oda H, Nakamura K, Kuga Y, Uchida S, Kawaguchi H. Involvement of fibroblast growth factor-2 in joint destruction of rheumatoid arthritis patients. Rheumatology (Oxford) 1999;38:714–20.
35. Clements KM, Price JS, Chambers MG, Visco DM, Poole AR, Mason RM. Gene deletion of either interleukin-1β, interleukin-1β–converting enzyme, inducible nitric oxide synthase, or stromelysin 1 accelerates the development of knee osteoarthritis in mice after surgical transection of the medial collateral ligament and partial medial meniscectomy. Arthritis Rheum 2003;48:3452–63.
36. D'Angelo M, Yan Z, Nooreyazdan M, Pacifici M, Sarment DS, Billings PC, et al. MMP-13 is induced during chondrocyte hypertrophy. J Cell Biochem 2000;77:678–93.
37. Jimenez MJ, Balbin M, Alvarez J, Komori T, Bianco P, Holmbeck K, et al. A regulatory cascade involving retinoic acid, Cbfa1, and matrix metalloproteinases is coupled to the development of a process of perichondrial invasion and osteogenic differentiation during bone formation. J Cell Biol 2001;155:1333–44.
38. Ziros PG, Gil AP, Georgakopoulos T, Habeos I, Kletsas D, Basdra EK, et al. The bone-specific transcriptional regulator Cbfa1 is a target of mechanical signals in osteoblastic cells. J Biol Chem 2002;277:23934–41.
39. Costessi A, Pines A, D'Andrea P, Romanello M, Damante G, Cesaratto L, et al. Extracellular nucleotides activate Runx2 in the osteoblast-like HOBIT cell line: a possible molecular link between mechanical stress and osteoblasts' response. Bone 2005;36:418–32.
40. Wong M, Siegrist M, Goodwin K. Cyclic tensile strain and cyclic hydrostatic pressure differentially regulate expression of hypertrophic markers in primary chondrocytes. Bone 2003;33:685–93.
41. Shimoaka T, Kamekura S, Chikuda H, Hoshi K, Chung UI, Akune T, et al. Impairment of bone healing by insulin receptor substrate-1 deficiency. J Biol Chem 2004;279:15314–22.
42. Radin EL, Rose RM. Role of subchondral bone in the initiation and progression of cartilage damage. Clin Orthop Relat Res 1986;213:34–40.
43. Burr DB. The importance of subchondral bone in osteoarthrosis [review]. Curr Opin Rheumatol 1998;10:256–62.
44. Glasson SS, Askew R, Sheppard B, Carito B, Blanchet T, Ma HL, et al. Deletion of active ADAMTS5 prevents cartilage degradation in a murine model of osteoarthritis. Nature 2005;434:644–8.
45. Stanton H, Rogerson FM, East CJ, Golub SB, Lawlor KE, Meeker CT, et al. ADAMTS5 is the major aggrecanase in mouse cartilage in vivo and in vitro. Nature 2005;434:648–52.
46. Wang X, Manner PA, Horner A, Shum L, Tuan RS, Nuckolls GH. Regulation of MMP-13 expression by RUNX2 and FGF2 in osteoarthritic cartilage. Osteoarthritis Cartilage 2004;12:963–73.
47. Mundlos S, Otto F, Mundlos C, Mulliken JB, Aylsworth AS, Albright S, et al. Mutations involving the transcription factor CBFA1 cause cleidocranial dysplasia. Cell 1997;89:773–9.
48. Otto F, Kanegane H, Mundlos S. Mutations in the RUNX2 gene in patients with cleidocranial dysplasia [review]. Hum Mutat 2002;19:209–16.

J Bone Miner Metab (2006) 24:95–99
DOI 10.1007/s00774-005-0653-0

MINI REVIEW

Fumitaka Kugimiya* · Shinsuke Ohba · Kozo Nakamura
Hiroshi Kawaguchi · Ung-il Chung

Physiological role of bone morphogenetic proteins in osteogenesis

Received: October 8, 2005 / Accepted: October 20, 2005

Key words bone morphogenetic protein · hypertrophic chondrocyte · bone formation · osteoblast

Introduction

Bone morphogenetic proteins (BMPs) are members of secreted signaling proteins that belong to the transforming growth factor-β superfamily. BMPs were originally identified as molecules that induced ectopic bone formation when implanted into rodent muscles [1,2]. In this process, mesenchymal precursor cells condense and differentiate into two distinct tissues, namely the cartilage template and the surrounding perichondrium. Subsequently, chondrocytes in the cartilage template undergo a program of proliferation, cell cycle arrest, hypertrophy, calcification, and ultimately cell death. Ossification of the calcified matrix around the hypertrophic layer occurs upon vascularization and the recruitment of osteoblasts to the site [3]. In accordance with such in vivo effects, BMPs have been shown to regulate osetoblast differentiation in vitro [4].

BMPs bind to a characteristic pair of type I and II transmembrane serine/threonine kinase receptors (Fig. 1). They first bind to the type II receptor, which phosphorylates the GS domain of the type I receptor. The activated type I receptor subsequently recruits and phosphorylates the transcription factors Smad1, Smad5, and Smad8 (R-Smads) through the GS domain. R-Smads then physically associate with Smad4 (Co-Smad), translocate into the nucleus, and activate the target genes in concert with other coactivators. Smad6 blocks BMP signaling by inhibiting the phosphorylation of the BMP-dependent R-Smads by the BMP type I receptors [5,6].

F. Kugimiya · S. Ohba · U. Chung (✉)
Division of Tissue Engineering, Faculty of Medicine, University of Tokyo, 7-3-1 Hongo, Bunkyo-ku, Tokyo 113-8655, Japan
Tel. +81-3-3815-5411 (ext. 37014); Fax +81-3-3818-4082
e-mail: uichung-tky@umin.ac.jp

F. Kugimiya · K. Nakamura · H. Kawaguchi
Division of Sensory and Motor System Medicine, University of Tokyo, Tokyo, Japan

*F. Kugimiya is a recipient of the JSBMR Encouragement Award 2004

Skeletal phenotypes of BMP knockout mice

Because BMP2, 3, 4, 5, 6, 7, and GDF5 are expressed in the developing skeletal elements [7], these BMPs may be involved in skeletogenesis. To clarify the physiological roles of BMPs, a number of BMP knockout mice were generated (Table 1). Briefly, homozygous *Bmp2*-deficient (*Bmp2*–/–) or *Bmp*4-deficient (*Bmp4*–/–) mice are embryonically lethal before the onset of skeletogenesis [8,9]. Twelve percent of heterozygous *Bmp4*+/– mice exhibit preaxial polydactyly. *Bmp*3–/– mice exhibit increased bone density [10]. *Short ear* mice, which are caused by a naturally occurring mutation in the *Bmp5* gene, have many anatomical abnormalities: reduced ear size, reduction in body size, reduction in the number of ribs, misshapen xiphoid appendix, hydronephrosis, and lung abnormalities [11]. *Bmp6*–/– mice have no skeletal patterning defects except a mild delay in sternum ossification that can be traced to the formation of mesenchymal condensation [12]. *Bmp7*–/– mice have patterning abnormalities in the hind limbs. However, histological analysis failed to detect any other abnormalities in osteoblast differentiation [13]. Brachypodism is a spontaneously occurring phenotype caused by a mutation in the *Gdf5* gene, characterized by a reduction in the length of the long bones and the replacement of two bones in most digits by a single skeletal element [14]. A generation of mice harboring mutations in two different BMP genes adds little to the knowledge of physiological bone formation (see Table 1) [15–21]. Thus, all naturally occurring or genetically engineered mice deficient in BMPs reported to date are either normal, exhibit abnormalities in skeletal patterning, or die during early embryonic development, and thus provide no information on the physiological role of endogenous BMPs in bone formation [7].

Table 1. Information from BMP knockout mice

BMP2–/–	Embryonically lethal, small allantois, lack of amnion
BMP3–/–	Increased bone density
BMP4+/–	Preaxial polydactyly of hindlimb, cystic kidney
BMP4–/–	Embryonically lethal, lack of allantois, heart defect
BMP5–/–	Short ear mice, abnormality of rib cage
BMP6–/–	Delayed sternum ossification
BMP7–/–	Abnormality of rib cage, polydactyly
BMP8a–/–	Defect in spermatogenesis
BMP8b–/–	Defect in spermatogenesis
BMP11–/–	Abnormality of A–P patterning of axial skeleton
BMP12–/–	Hydrocephalic abnormality
BMP15–/–	Defect in oogenesis
GDF5–/–	Brachypodism, shortened limbs, reduced digit bones
GDF8–/–	Skeletal muscle hypertrophy
GDF9–/–	Defect in oogenesis
BMP2+/–; BMP4+/–	Fewer primordial germ cells than BMP2+/– or BMP4+/–
BMP2+/–; BMP6–/–	Reduction in bone formation due to osteoblast dysfunction
BMP2+/–; BMP7+/–	No skeletal abnormality
BMP4+/–; BMP7+/–	Skeletal defect in rib cage, polydactyly
BMP5–/–; BMP6–/–	Almost the same as BMP5–/–
BMP5+/–; BMP7+/–	No skeletal abnormality
BMP5–/–; BMP7–/–	Embryonically lethal, defect in cardiac cushion and septation
BMP5–/–; GDF5–/–	Combination of BMP5–/– and GDF5–/–
BMP6–/–; BMP7–/–	Embryonically lethal, lack of allantois, heart defect
BMP7+/–; BMP8a–/–	More severe defects in spermatogenesis than BMP8a–/–
BMP8a+/–; BMP8b+/–	Defects in spermatogenesis and epididymis

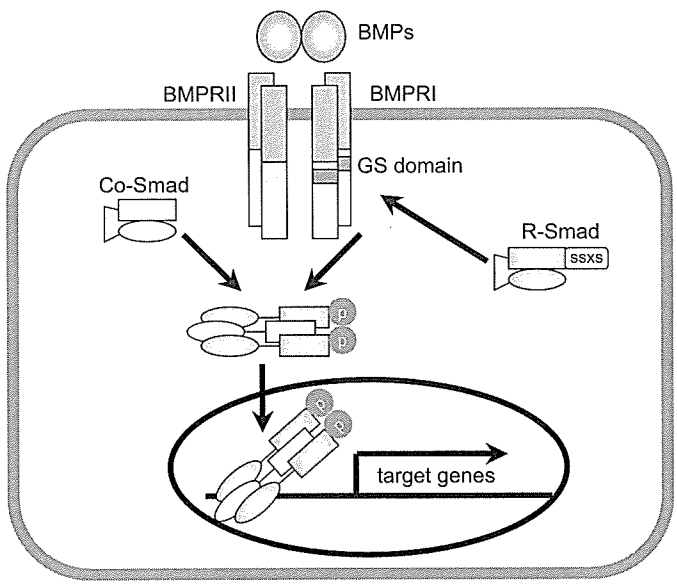

Fig. 1. BMP/Smad signaling pathway. BMPs bind to type I and type II receptors that are membrane-bound serine/threonine kinase receptors. Upon ligand binding, type II receptor phosphorylates the GS domain of the type I receptor, and type I receptor induces phosphorylation of R-Smads. Phosphorylated R-Smads form complexes with Co-Smad, and translocate into the nucleus

Induction of bone formation by hypertrophic chondrocytes

The vertebrate skeleton is derived from three distinct embryonic lineages: neural crest cells, paraxial mesoderm, and lateral plate mesoderm. Cells of these lineages proliferate and migrate into distinct mesenchymal condensations at the sites of future elements. Subsequently, they follow two distinct ways of bone formation: intramembranous and endochondral [3]. During intramembranous bone formation, condensed mesenchymal cells differentiate directly into osteoblasts. Most craniofacial bones and clavicles are formed through this process. Most of the bones are formed through the latter process, which is characterized by the replacement of a cartilage mold by bone and bone marrow [22]. In endochondral bone formation, there are several pieces of evidence that show that hypertrophic chondrocytes induce bone formation in adjacent tissues. First, bone formation always occurs in locations adjacent to the hypertrophic chondrocytes [23]. The primary spongiosa and bone collar are formed around the hypertrophic chondrocytes. This rule applies to all endochondral bones, large or small, without exception. Second, in mice lacking the *parathyroid hormone (Pth)-related peptode (Pthrp)* gene or its receptor, the *Pth/Pthrp receptor* (*Ppr*) gene, the regulation of hypertrophy is disturbed, and ectopic chondrocyte hypertrophy and ectopic bone formation appear [24–26]. Third, both the hypertrophy of chondrocytes and the formation of bone collar and primary spongiosa are suppressed in transgenic mice expressing the constitutively active *Ppr* under the control of the chondrocyte-specific type II collagen promoter (Col II *Ppr* transgenic mice) [27]. Furthermore, by the introduction of the Col II *Ppr* transgene, both the ectopic hypertrophy and the ectopic bone formation seen in *Pthrp–/–* mice are reversed [23]. Thus, the chondrocyte-specific manipulation of PTHrP signaling influences the appearance of ectopic bone formation. Fourth, in the growth plate of *Ppr–/–/WT* chimeric mice, ectopic bone collars are formed near clusters of ectopic prehypertrophic/hypertrophic chondrocytes [23]. Thus, during endochondral bone formation, hypertrophic chondrocytes in the growth plate link chondrogenesis to

osteogenesis by inducing osteogenesis in adjacent perichondrium and primary spongiosa.

Hypertrophic chondrocytes express a number of growth factors, cytokines, and matrix proteins. Among them, Indian hedgehog (Ihh) has been proven to be indispensable for osteogenesis by hypertrophic chondrocytes [23,28]. However, Ihh alone cannot induce bone formation [29], suggesting that other factors secreted from hypertrophic chondrocytes may also be necessary for osteogenesis. Because some BMPs can induce ectopic bone formation when implanted into rodent muscles and promote osteoblast differentiation in vitro, they are strong candidates for osteogenic factors secreted from hypertrophic chondrocytes.

BMP subtypes expressed by hypertrophic chondrocytes

Because hypertrophic chondrocytes induce bone formation in the primary spongiosa and the perichondrium during endochondral bone development, BMPs that are important for physiological bone formation are likely to be expressed by hypertrophic chondrocytes. BMP2, 3, 4, 5, 6, 7, and GDF5 are known to be expressed in the growth plate [7,12]. BMP2 is expressed in the hypertrophic chondrocytes, the perichondrium, and the developing joints. Expression of BMP3 is detected in the perochondrium along the shaft, but not surrounding the epiphyses. BMP4 transcripts are detected in the cells of the perichondrium and the transition zone adjacent to the mature hypertrophic chondrocytes. BMP5 is expressed in the perichondrium. BMP6 expression is localized to the hypertrophic chondrocytes and joints. Expression of BMP7 is detected in the proliferative chondrocytes and the inner perichondrium. These reports indicate that the main BMP subtypes expressed by the hypertrophic chondrocytes are BMP2 and BMP6 [12,30].

Bmp2+/–; *Bmp6*–/– mice exhibited growth retardation with proportional growth plates

As is the case with the other BMPs, however, there is no direct evidence that BMP2 and BMP6 are essential for physiological bone formation, because *Bmp2*–/– mice die at an early embryonic stage [8], and *Bmp6*–/– mice show no skeletal abnormality except for a slight delay in the ossification of the sternum [12]. Because there may be genetic redundancy between BMP2 and BMP6 in the regulation of bone formation, compound knockout mice lacking one allele of the *Bmp2* gene and both alleles of the *Bmp6* gene (*Bmp2*+/–; *Bmp6*–/–) were generated and the effect on bone formation was analyzed [30].

Although BMPs are known to play important roles in skeletal patterning during embryonic development, there was no apparent abnormality of skeletal patterning in *Bmp2*+/–; *Bmp6*–/– mice. In contrast, there was growth retardation in *Bmp2*+/–; *Bmp6*–/– mice. The size of the *Bmp2*+/–; *Bmp6*–/– growth plate was smaller than that of the WT, but the proportions of the distinct layers of growth plate chondrocytes (periarticular proliferative, columnar proliferative, and hypertrophic) showed no significant differences. Although several lines of evidence indicate that BMPs promote chondrocyte hypertrophy, *Bmp2*+/–; *Bmp6*–/– mice did not show a significant difference in chondrocyte differentiation.

Impaired bone formation due to osteoblast dysfunction in *Bmp2*+/–; *Bmp6*–/– mice

As for bone formation, the trabecular bone volume and cortical thickness were significantly reduced in *Bmp2*+/–; *Bmp6*–/– mice. Bone histomorphometric analysis showed that bone volume was decreased by 31% compared with that of the WT. Regarding the parameters of bone formation, there was a significant reduction in mineral apposition rate and bone formation rate per bone surface, but little difference in osteoblast number. On the other hand, the parameters of bone resorption were normal. These data suggest that bone loss in *Bmp2*+/–; *Bmp6*–/– mice was caused by the inhibition of bone formation due to an impairment of osteoblast function. Urinary deoxypyridinoline, a marker for bone resorption, showed little difference between the two groups.

Fracture healing recapitulates some aspects of the intramembranous and endochondral bone development [31], and the abnormalities of such development are sometimes exaggerated in fracture healing. The endochondral, not the intramembranous, bone formation was defective in *Bmp2*+/–; *Bmp6*–/– mice. In *Bmp2*+/–; *Bmp6*–/– mice, a massive cartilaginous callus persisted, which contained hypertrophic chondrocytes. The hypertrophic differentiation of chondrocytes was similar between WT and *Bmp2*+/–; *Bmp6*–/– mice, suggesting that the bone induction ability of the hypertrophic chondrocytes was impaired in *Bmp2*+/–; *Bmp6*–/– mice.

Comparison of *Bmp2*+/–; *Bmp6*–/– mice and mice deficient in the BMP signaling cascade

Recently, transgenic mice expressing a dominant-negative form of *Bmp receptor 1b* (*Bmpr-1b*) under the control of the type I collagen promoter were generated, and they closely resembled *Bmp2*+/–; *Bmp6*–/– mice [32]. They were smaller than the WT mice and showed impairment of postnatal bone formation with the number of osteoblasts and the parameters of bone resorption unchanged, suggesting that osteoblast function was impaired. In addition, transgenic mice lacking the *Bmp receptor 1a* (*Bmpr-1a*) specifically in osteoblasts using the Cre/loxP system under the control of the osteocalcin 2 promoter also exhibited low bone mass due to impaired osteoblast function [33]. Noggin

is a secreted glycoprotein and acts as a BMP antagonist. Noggin binds to BMP2, 4, 5, 6, and 7 and inhibits their binding to the BMP receptors. Transgenic mice expressing *Noggin* under the control of the osteocalcin promoter exhibited a reduction in the trabecular bone volume and the bone formation rate, but not in the number of osteoblasts [34,35]. Smurf1 is a HECT domain ubiquitin E3 ligase and inhibits BMP signaling by inducing the degradation of R-Smads and BMP receptors. A deficiency of *Smurf1* in mice showed an increase in bone mass due to the enhanced activities of osteoblasts [36], and transgenic mice expressing *Smurf1* under the control of the type I collagen promoter exhibited osteopenia [37]. The bone phenotypes of these genetically manipulated mice, in which the osteoblasts could not transduce normal BMP signaling, were similar to those of *Bmp2+/–*; *Bmp6–/–* mice. These data support our hypothesis that BMP2 and BMP6 act on osteoblasts to induce normal bone formation.

References

1. Wozney JM, Rosen V, Celeste AJ, Mitsock LM, Whitters MJ, Kriz RW, Hewick RM, Wang EA (1988) Novel regulators of bone formation: molecular clones and activities. Science 242:1528–1534
2. Urist MR (1965) Bone: formation by autoinduction. Science 150: 893–899
3. Kronenberg HM (2003) Developmental regulation of the growth plate. Nature 423:332–336
4. Kawabata M, Miyazono K (2000) Bone morphogenetic proteins. In: Canalis MDE (ed) Skeletal Growth Factors. Lippincott Williams & Wilkins, Philadelphia, 269–290
5. Miyazono K, Maeda S, Imamura T (2005) BMP receptor signaling: transcriptional targets, regulation of signals, and signaling cross-talk. Cytokine Growth Factor Rev 16:251–263
6. Kawabata M, Imamura T, Miyazono K (1998) Signal transduction by bone morphogenetic proteins. Cytokine Growth Factor Rev 9:49–61
7. Karsenty G (2000) Bone morphogenetic proteins and skeletal and nonskeletal development. In: Canalis MDE (ed) Skeletal Growth Factors. Lippincott Williams & Wilkins, Philadelphia, 291–310
8. Zhang H, Bradley A (1996) Mice deficient for BMP2 are nonviable and have defects in amnion/chorion and cardiac development. Development 122:2977–2986
9. Winnier G, Blessing M, Labosky PA, Hogan BL (1995) Bone morphogenetic protein-4 is required for mesoderm formation and patterning in the mouse. Genes Dev 9:2105–2116
10. Daluiski A, Engstrand T, Bahamonde ME, Gamer LW, Agius E, Stevenson SL, Cox K, Rosen V, Lyons KM (2001) Bone morphogenetic protein-3 is a negative regulator of bone density. Nat Genet 27:84–88
11. Kingsley DM, Bland AE, Grubber JM, Marker PC, Russell LB, Copeland NG, Jenkins NA (1992) The mouse short ear skeletal morphogenesis locus is associated with defects in a bone morphogenetic member of the TGF beta superfamily. Cell 71:399–410
12. Solloway MJ, Dudley AT, Bikoff EK, Lyons KM, Hogan BL, Robertson EJ (1998) Mice lacking Bmp6 function. Dev Genet 22:321–339
13. Luo G, Hofmann C, Bronckers AL, Sohocki M, Bradley A, Karsenty G (1995) BMP-7 is an inducer of nephrogenesis, and is also required for eye development and skeletal patterning. Genes Dev 9:2808–2820
14. Storm EE, Huynh TV, Copeland NG, Jenkins NA, Kingsley DM, Lee SJ (1994) Limb alterations in brachypodism mice due to mutations in a new member of the TGF beta-superfamily. Nature 368: 639–643
15. Ying Y, Zhao GQ (2001) Cooperation of endoderm-derived BMP2 and extraembryonic ectoderm-derived BMP4 in primordial germ cell generation in the mouse. Dev Biol 232:484–492
16. Katagiri T, Boorla S, Frendo JL, Hogan BL, Karsenty G (1998) Skeletal abnormalities in doubly heterozygous Bmp4 and Bmp7 mice. Dev Genet 22:340–348
17. Solloway MJ, Robertson EJ (1999) Early embryonic lethality in Bmp5;Bmp7 double mutant mice suggests functional redundancy within the 60A subgroup. Development 126:1753–1768
18. Storm EE, Kingsley DM (1996) Joint patterning defects caused by single and double mutations in members of the bone morphogenetic protein (BMP) family. Development 122:3969–3979
19. Kim RY, Robertson EJ, Solloway MJ (2001) Bmp6 and Bmp7 are required for cushion formation and septation in the developing mouse heart. Dev Biol 235:449–466
20. Zhao GQ, Chen YX, Liu XM, Xu Z, Qi X (2001) Mutation in Bmp7 exacerbates the phenotype of Bmp8a mutants in spermatogenesis and epididymis. Dev Biol 240:212–222
21. Zhao GQ, Liaw L, Hogan BL (1998) Bone morphogenetic protein 8A plays a role in the maintenance of spermatogenesis and the integrity of the epididymis. Development 125:1103–1112
22. Chung UI (2004) Essential role of hypertrophic chondrocytes in endochondral bone development. Endocr J 51:19–24
23. Chung UI, Schipani E, McMahon AP, Kronenberg HM (2001) Indian hedgehog couples chondrogenesis to osteogenesis in endochondral bone development. J Clin Invest 107:295–304
24. Karaplis AC, Luz A, Glowacki J, Bronson RT, Tybulewicz VL, Kronenberg HM, Mulligan RC (1994) Lethal skeletal dysplasia from targeted disruption of the parathyroid hormone-related peptide gene. Genes Dev 8:277–289
25. Amizuka N, Henderson JE, Hoshi K, Warshawsky H, Ozawa H, Goltzman D, Karaplis AC (1996) Programmed cell death of chondrocytes and aberrant chondrogenesis in mice homozygous for parathyroid hormone-related peptide gene deletion. Endocrinology 137:5055–5067
26. Lanske B, Karaplis AC, Lee K, Luz A, Vortkamp A, Pirro A, Karperien M, Defize LH, Ho C, Mulligan RC, Abou-Samra AB, Juppner H, Segre GV, Kronenberg HM (1996) PTH/PTHrP receptor in early development and Indian hedgehog-regulated bone growth. Science 273:663–666
27. Schipani E, Lanske B, Hunzelman J, Luz A, Kovacs CS, Lee K, Pirro A, Kronenberg HM, Juppner H (1997) Targeted expression of constitutively active receptors for parathyroid hormone and parathyroid hormone-related peptide delays endochondral bone formation and rescues mice that lack parathyroid hormone-related peptide. Proc Natl Acad Sci USA 94:13689–13694
28. Long F, Chung UI, Ohba S, McMahon J, Kronenberg HM, McMahon AP (2004) Ihh signaling is directly required for the osteoblast lineage in the endochondral skeleton. Development 131:1309–1318
29. Long F, Zhang XM, Karp S, Yang Y, McMahon AP (2001) Genetic manipulation of hedgehog signaling in the endochondral skeleton reveals a direct role in the regulation of chondrocyte proliferation. Development 128:5099–5108
30. Kugimiya F, Kawaguchi H, Kamekura S, Chikuda H, Ohba S, Yano F, Ogata N, Katagiri T, Harada Y, Azuma Y, Nakamura K, Chung UI (2005) Involvement of endogenous bone morphogenetic protein (BMP)2 and BMP6 in bone formation. J Biol Chem 280:35704–35712
31. Vortkamp A, Pathi S, Peretti GM, Caruso EM, Zaleske DJ, Tabin CJ (1998) Recapitulation of signals regulating embryonic bone formation during postnatal growth and in fracture repair. Mech Dev 71:65–76
32. Zhao M, Harris SE, Horn D, Geng Z, Nishimura R, Mundy GR, Chen D (2002) Bone morphogenetic protein receptor signaling is necessary for normal murine postnatal bone formation. J Cell Biol 157:1049–1060
33. Mishina Y, Starbuck MW, Gentile MA, Fukuda T, Kasparcova V, Seedor JG, Hanks MC, Amling M, Pinero GJ, Harada S, Behringer RR (2004) Bone morphogenetic protein type IA receptor signaling regulates postnatal osteoblast function and bone remodeling. J Biol Chem 279:27560–27566
34. Wu XB, Li Y, Schneider A, Yu W, Rajendren G, Iqbal J, Yamamoto M, Alam M, Brunet LJ, Blair HC, Zaidi M, Abe E

(2003) Impaired osteoblastic differentiation, reduced bone formation, and severe osteoporosis in noggin-overexpressing mice. J Clin Invest 112:924–934
35. Devlin RD, Du Z, Pereira RC, Kimble RB, Economides AN, Jorgetti V, Canalis E (2003) Skeletal overexpression of noggin results in osteopenia and reduced bone formation. Endocrinology 144:1972–1978
36. Yamashita M, Ying SX, Zhang GM, Li C, Cheng SY, Deng CX, Zhang YE (2005) Ubiquitin ligase Smurf1 controls osteoblast activity and bone homeostasis by targeting MEKK2 for degradation. Cell 121:101–113
37. Zhao M, Qiao M, Harris SE, Oyajobi BO, Mundy GR, Chen D (2004) Smurf1 inhibits osteoblast differentiation and bone formation in vitro and in vivo. J Biol Chem 279:12854–12859

nature medicine

LETTERS

Carminerin contributes to chondrocyte calcification during endochondral ossification

Takashi Yamada[1], Hirotaka Kawano[1], Yu Koshizuka[1], Toru Fukuda[2], Kimihiro Yoshimura[2], Satoru Kamekura[1], Taku Saito[1], Toshiyuki Ikeda[1], Yosuke Kawasaki[1], Yoshiaki Azuma[3], Shiro Ikegawa[4], Kazuto Hoshi[1], Ung-il Chung[1], Kozo Nakamura[1], Shigeaki Kato[2] & Hiroshi Kawaguchi[1]

Endochondral ossification is an essential process not only for physiological skeletal development and growth, but also for pathological disorders. We recently identified a novel cartilage-specific molecule, carminerin (also known as cystatin 10 and encoded by *Cst10*), which is upregulated in synchrony with cartilage maturation and stimulates the later differentiation of cultured chondrocytes[1]. Although carminerin-deficient (*Cst10*$^{-/-}$) mice developed and grew normally, they had a microscopic decrease in the calcification of hypertrophic chondrocytes at the growth plate. When we created experimental models of pathological endochondral ossification, we observed suppression of chondrocyte calcification during formation of osteoarthritic osteophytes, age-related ectopic ossification and healing of bone fractures in *Cst10*$^{-/-}$ mice. Cultured *Cst10*$^{-/-}$ chondrocytes showed a reduction in calcification with activation of an SRY site in the promoter of the gene encoding nucleotide pyrophosphatase phosphodiesterase 1 (NPP1, encoded by *Enpp1*). Functional NPP1 is required for carminerin deficiency to suppress the pathological endochondral ossifications listed above. Carminerin is the first cartilage-specific protein that contributes to chondrocyte calcification during endochondral ossification under physiological and pathological conditions through the transcriptional inhibition of NPP1.

We generated *Cst10*$^{-/-}$ mice by homologous recombination in mouse embryonic stem cells using a targeting vector to replace exon 1 with the phosphoglycerate kinase-neomycin (PGKneo) cassette (**Fig. 1a**). Inbreeding of heterozygous *Cst10*$^{+/-}$ mice yielded *Cst10*$^{-/-}$ mice, as determined by Southern blot analysis, at the expected mendelian ratio (**Fig. 1b**). Neither *Cst10* transcripts nor carminerin protein was detected in the rib cartilage of *Cst10*$^{-/-}$ mice, confirming disruption of the *Cst10* gene (**Fig. 1c,d**). *Cst10*$^{-/-}$ mice developed and grew similarly to wild-type (*Cst10*$^{+/+}$) and *Cst10*$^{+/-}$ littermates without abnormalities of major organs (**Fig. 1e,f**).

Radiological analyses of femurs and tibiae in 8-week-old mice showed that *Cst10*$^{-/-}$ mice experienced decreases in trabecular bone volume mainly at the metaphysis, but not in cortical bone at the diaphysis, as compared to the wild-type littermates (**Fig. 2a,b** and **Supplementary Fig. 1** online). Histological examination of the proximal tibias indicated a decrease in trabecular bone volume beneath the growth plate of *Cst10*$^{-/-}$ mice (**Fig. 2c**). Although expression of carminerin was localized mainly in the wild-type hypertrophic chondrocytes, the columnar architecture, expression of type X collagen (Col X) and the entire width of the growth plate were comparable between wild-type and *Cst10*$^{-/-}$ mice, indicating that hypertrophic differentiation of chondrocytes was not affected by the carminerin deficiency (**Fig. 2c,d**). The width of the calcified layer and the number of calcified chondrocytes, as determined by von Kossa staining, however, were reduced (**Fig. 2c,d**). Bone volume in the *Cst10*$^{-/-}$ primary spongiosa just beneath the growth plate was significantly reduced ($P < 0.01$), with normal numbers of tartrate-resistant acid phosphatase (TRAP)-positive chondroclasts or osteoclasts, whereas the secondary spongiosa was not affected (**Fig. 2c,d** and **Supplementary Fig. 1**). In vertebral bodies that undergo less longitudinal growth by the thinner growth plate than femurs and tibiae, the histomorphometric parameters were comparable between the two genotypes in the growth plate and the primary and secondary spongiosa (**Supplementary Fig. 1**). These findings indicate that the decrease in trabecular bone adjacent to the growth plate of *Cst10*$^{-/-}$ long bones under physiological conditions resulted primarily from impairment of the calcification of hypertrophic chondrocytes, but not from the abnormality of cartilage resorption by chondroclasts or bone formation by osteoblasts.

We then examined the involvement of carminerin in pathological endochondral ossification by using experimental models involving wild-type and *Cst10*$^{-/-}$ littermates. First, we investigated the role of carminerin in the pathogenesis of osteoarthritis by inducing instability in the mouse knee joint[2]. The joint cartilage destruction was similarly visible at the posterior of the tibias (**Fig. 3a**) in both genotypes. The

[1]Department of Sensory & Motor System Medicine, Faculty of Medicine, University of Tokyo, Hongo 7-3-1, Bunkyo, Tokyo 113-8655, Japan. [2]Institute of Molecular and Cellular Biosciences, University of Tokyo, Yayoi 1-1-1, Bunkyo, Tokyo 113-0032, Japan. [3]Teijin Institute for Biomedical Research, Asahigaoka 4-3-2, Hino, Tokyo 191-8512, Japan. [4]Institute of Physical and Chemical Research (RIKEN), Shirokanedai, Minato, Tokyo 106-8639, Japan. Correspondence should be addressed to H.K. (kawaguchi-ort@h.u-tokyo.ac.jp).

Received 1 January; accepted 7 April; published online 7 May 2006; doi:10.1038/nm1409

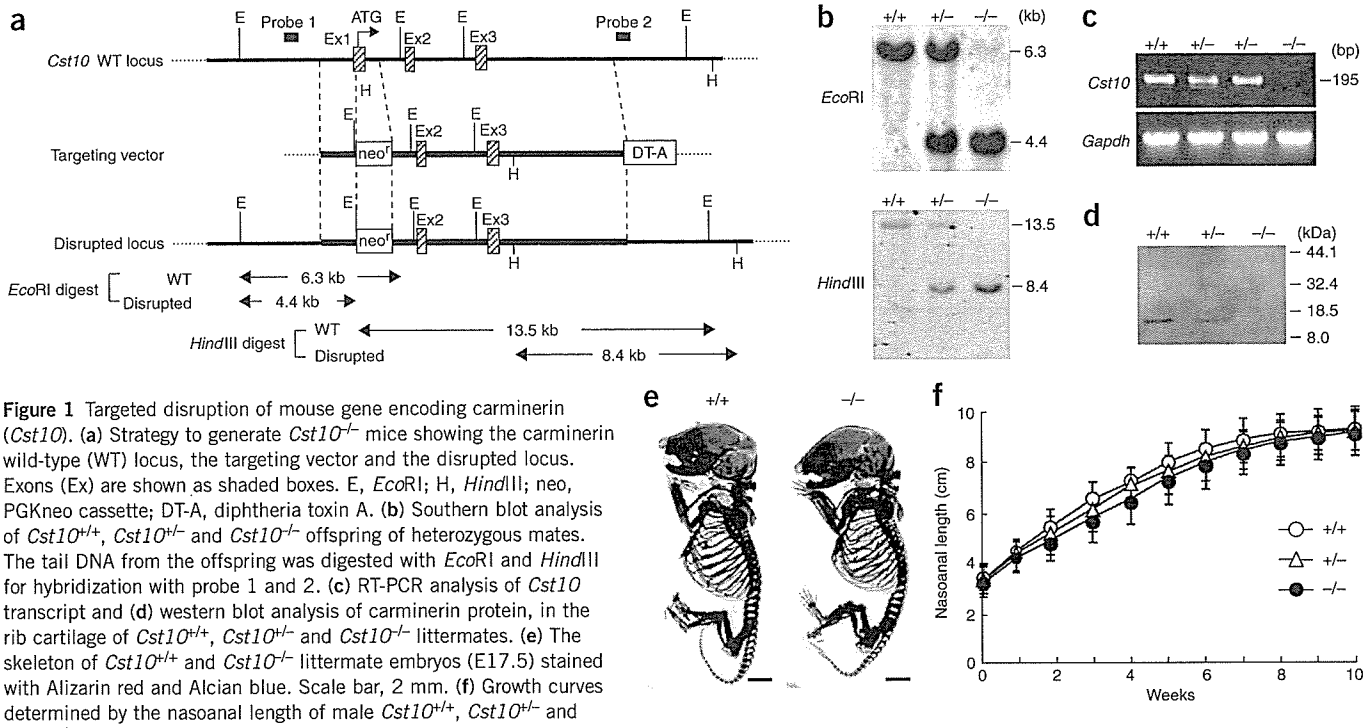

Figure 1 Targeted disruption of mouse gene encoding carminerin (*Cst10*). (**a**) Strategy to generate *Cst10*$^{-/-}$ mice showing the carminerin wild-type (WT) locus, the targeting vector and the disrupted locus. Exons (Ex) are shown as shaded boxes. E, *Eco*RI; H, *Hind*III; neo, PGKneo cassette; DT-A, diphtheria toxin A. (**b**) Southern blot analysis of *Cst10*$^{+/+}$, *Cst10*$^{+/-}$ and *Cst10*$^{-/-}$ offspring of heterozygous mates. The tail DNA from the offspring was digested with *Eco*RI and *Hind*III for hybridization with probe 1 and 2. (**c**) RT-PCR analysis of *Cst10* transcript and (**d**) western blot analysis of carminerin protein, in the rib cartilage of *Cst10*$^{+/+}$, *Cst10*$^{+/-}$ and *Cst10*$^{-/-}$ littermates. (**e**) The skeleton of *Cst10*$^{+/+}$ and *Cst10*$^{-/-}$ littermate embryos (E17.5) stained with Alizarin red and Alcian blue. Scale bar, 2 mm. (**f**) Growth curves determined by the nasoanal length of male *Cst10*$^{+/+}$, *Cst10*$^{+/-}$ and *Cst10*$^{-/-}$ mice. Data are expressed as mean ± s.e.m. for 15 mice per group. Females also showed similar skeletal development and growth in all genotypes.

carminerin expression was colocalized with Col X in the wild-type hypertrophic chondrocytes adjacent to the osteophyte (**Fig. 3b**). Although the hypertrophic differentiation of chondrocytes was not affected by the carminerin deficiency (**Fig. 3a**), osteophyte formation at the posterior of the tibias was significantly decreased (**Fig. 3a,c**). These findings confirmed by quantification by the Mankin grading score[3] and the osteophyte volume (**Fig. 3d**) indicate that carminerin produced in hypertrophic chondrocytes as a result of mechanical stress contributes to osteophyte formation through chondrocyte calcification, without affecting cartilage destruction or chondrocyte hypertrophy.

Similar findings were observed in ectopic ossification of the patellar ligament and the Achilles tendon with aging (**Supplementary Methods** online), which was significantly decreased by the carminerin deficiency ($P < 0.05$; **Supplementary Fig. 2** online). The colocalization of Col X and carminerin adjacent to the ectopic ossification indicates the involvement of carminerin-expressing hypertrophic chondrocytes in this disorder as well (**Supplementary Fig. 2**).

We further examined the involvement of carminerin in bone fracture healing at the midshaft of tibias[4,5]. *Cst10*$^{-/-}$ mice showed a bone gap upon X-ray 3 weeks after the fracture, with substantial formation of cartilaginous callus but impaired calcification, especially at the central area (**Fig. 4a**). Again, carminerin was expressed in the wild-type chondrocytes adjacent to the calcified callus. The time course of bone mineral content (BMC) showed that calcification in the central one-third portion, but not in the peripheral two-thirds portion, was significantly reduced during the endochondral ossification period (2–7 weeks after fracture) in the *Cst10*$^{-/-}$ callus, although bone union was eventually achieved from the *Cst10*$^{-/-}$ small callus through unaffected bone formation and remodeling thereafter (**Fig. 4b**). This model also indicates that the carminerin deficiency impaired endochondral ossification, but not intramembranous ossification or osteoblastic bone formation.

The effects of carminerin deficiency on endochondral ossification under the pathological conditions above were more obvious than those under physiological conditions, which showed only a microscopic change. The phenotype of the physiological *Cst10*$^{-/-}$ growth plate was milder than that seen in other disorders such as vitamin A deficiency, which causes not only impaired chondrocyte calcification but also insufficient resorption of unmineralized cartilage by chondroclasts, leading to a suppressed skeletal growth[6]. The difference may be caused by operation of compensatory mechanisms for endochondral ossification, including osteoblastic bone formation and remodeling unaffected by the carminerin deficiency, which are sufficient to compensate for the deficiency under physiological conditions, but not so under pathological conditions.

Carminerin was originally called cystatin 10 because its amino acid sequence contained similarity to the cystatin protein family; however, our examination has not detected legitimate cystatin activity, which inhibits cysteine proteinases (**Supplementary Table 1** and **Supplementary Methods** online). We therefore renamed this protein carminerin after 'cartilage mineralization'. To elucidate the actual mechanism of carminerin action on endochondral ossification, we compared *ex vivo* cultures of chondrocytes isolated from the growth plates of the wild-type and *Cst10*$^{-/-}$ tibias (**Supplementary Methods**). Although chondrocyte proliferation and differentiation were similar between the two genotypes, chondrocyte calcification was suppressed in the *Cst10*$^{-/-}$ culture (**Supplementary Fig. 3** online), indicating a cell-autonomous effect. In contrast, *ex vivo* cultures of primary osteoblasts obtained from wild-type and *Cst10*$^{-/-}$ calvariae confirmed that these cells do not express carminerin, so that there was no difference of bone formation by osteoblasts in this bone type (**Supplementary Fig. 3**).

As inorganic pyrophosphate (PPi) is known to be a crucial inhibitor of calcification[7], we compared the expression of a few molecules that